International Journal of Non-Linear Mechanics 118 (2020) 103302

Contents lists available at ScienceDirect

International Journal of Non-Linear Mechanics

journal homepage: www.elsevier.com/locate/nlm

Analysis of flexible elastic–plastic plates/shells behaviour under coupled mechanical/thermal fields and one-sided corrosion wear

J. Awrejcewicz [a,*], A.V. Krysko [b,c], E.Yu. Krylova [d], T.Y. Yaroshenko [e], M.V. Zhigalov [e], V.A. Krysko [e]

[a] Department of Automation, Biomechanics and Mechatronics, Lodz University of Technology, 1/15 Stefanowskiego St., 90-924 Lodz, Poland
[b] Department of Applied Mathematics and Systems Analysis, Saratov State Technical University, 410054 Saratov, Politehnicheskaya 77, Russian Federation
[c] Cybernetic Institute, National Research Tomsk Polytechnic University, 634050 Tomsk, Lenin Avenue, 30, Russian Federation
[d] Department of Mathematical and Computer Modelling, Saratov State University, 43 Astrachanskay Str., 410054 Saratov, Russian Federation
[e] Department of Mathematics and Modelling, Saratov State Technical University, 77 Politehnicheskaya Str., 410054 Saratov, Russian Federation

ARTICLE INFO

Keywords:
Plates and shells
Vibration
Non-linearity
Temperature

ABSTRACT

Mathematical models of a non-linear shallow shell subjected to mechanical and temperature fields and one-sided corrosion wear are proposed. The governing equations are yielded by Hamilton's principle. The geometric and physical non-linearity follow the Föppl–Kármán approximation and the plastic deformation theory, respectively. Dolinskii and Gutman corrosion models as well as the Duhamel–Neumann model are implemented. The governing mixed-type PDEs are derived. The algorithm to solve the PDEs is based on the method of variational iterations (MVI) and linearization. Convergence of the developed procedure is proved. Theoretical considerations are validated by numerical results.

1. Introduction

Due to its importance, the problem of corrosion wear and damage has been reconsidered in recent years. Numerous metallic constructions and machines are subjected to aggressive chemical compounds in the atmosphere, rivers, and seas (ships/boats operating in water environments), in mining as well as in technological and working toxic/oxidable environments of different industries. The corrosion wear is harmful in shipbuilding, machine constructions, and other branches of industry. Interaction of metals with aggressive environments causes chemical reactions resulting in damage of mechanical constructions and qualitative change in their stress–strain state. The corrosion processes are non-invertible, and the corroded system cannot come back to its initial state. The occurred dynamic mechano-chemical regimes cause a change in parameters of the force (mechanical) load, which is accompanied by a change in the construction volume (thickness) as well as the occurrence of thermal stresses. Engineers and application-oriented researchers are focused on developing mechanical constructions able to work in the aggressive environment and in conditions of non-uniform and non-stationary heating (for instance, in air and rocket techniques, pipeline systems, micromechanical systems, etc.). Therefore, there is a need for updated and reliable modelling of those dynamical systems and reliable methods of their numerical solutions [1–15]. The state-of-the art regarding nonlinear shells vibration is reported in Ref. [16].

Since plates and shells are widely used in almost all industrial branches, their dynamical regimes, the interplay with the aggressive environment, and the yielded wear corrosion phenomena are challenging from the point of view of both theory and application.

Numerous metal structures used in the aircraft industry, ships and offshore structures, as well as chemical engineering, are subjected to both internal/external high-pressure and chemical action of the environments, and hence their damage is induced by mechanical stress, electrochemical corrosion, and mechano-chemical wear [17–21].

The problems of dynamics, durability, and stability of thin-walled structures, including high-pressure vessels, cylindrical pipes and tubes, bars, plates, and shells under stress-assisted wear and mechano-chemical corrosion are important in numerous branches of engineering.

Gutman et al. [21] proposed a method for detection of the critical time of stability loss in thin-walled high-pressure vessels under uniform corrosion from the inside. In the paper, the authors demonstrated how the critical time was estimated based on knowledge of the respective problem of the static stability loss for the vessel and the law of corrosion rate.

Then, Gutman et al. [22] carried out similar investigations of thin-walled cylindrical pipes with non-circular cross-section and variable

* Corresponding author.
E-mail addresses: awrejcew@p.lodz.pl (J. Awrejcewicz), anton.krysko@gmail.com (A.V. Krysko), Kat.Krylova@bk.ru (E.Yu. Krylova), tyyaroshenko@gmail.com (T.Y. Yaroshenko), zhigalovm@ya.ru (M.V. Zhigalov), tak@san.ru (V.A. Krysko).

https://doi.org/10.1016/j.ijnonlinmec.2019.103302
Received 23 July 2019; Received in revised form 4 October 2019; Accepted 6 October 2019
Available online 10 October 2019
0020-7462/

wall thickness along the directrix to non-homogeneous corrosion from the inside. The presented numerical results concerned the pipe of an elliptical cross-section.

Bergman et al. [23] investigated stability loss of thin-walled elastic circular cylindrical pipes under the simultaneous action of longitudinal forces and uniform corrosion from the outside. The critical time of stability loss was estimated for pipes made from steel and aluminium with different initial wall thickness.

Peng et al. [24] studied the influence of the interaction between multiple local wall thinning defects on strength of pipes subjected to different load conditions. A quantified index was introduced to measure the interaction between the occurred defects.

Pronina [25] analysed the uniform surface mechano-chemical corrosion of an elastic thick-walled cylindrical tube under internal and external pressure and a temperature field. However, the problem was strongly reduced to the first-order ordinary differential equation. Elishakoff et al. [26] investigated the durability of a bar under tension and corrosion. Closed-form formulae were derived for structural durability, and the obtained results were validated.

Eslami-Majd and Rahbar-Ranji [27] carried out free vibration analysis of stiffened/unstiffened pitted corroded plates. Corrosion patterns on the one-sided plates were studied for different plate frequencies and modes.

Pronina [28] derived an analytical solution for the equal-rate mechano-chemical wear of an ideal elastic–plastic thick-walled cylindrical tube under internal/external pressure. It was shown that the plastic zone propagation through the tube wall can be much greater than the length of the pure elastic stage.

Zhang et al. [29] conducted tensile tests under different loading conditions to study the corrosion phenomena of low carbon and low alloy steel with different microstructures in the NaCl solution. It was illustrated that steel exhibited more serious damage under the dynamic loading condition than under the static one and that dual phase steel underwent high sensitivity to mechano-chemical effect.

Sedova and Pronina [30] proposed an analytical solution for determining the optimal initial thickness of a spherical member under the conditions of double-side mechano-chemical corrosion. It was assumed that the corrosion rates were linearly dependent on the maximum stress and exponentially decaying with time.

Pronina et al. [31] compared two analytical solutions for the equal-rate mechano-chemical corrosion of the elastic spherical shells under external and internal stress. The corrosion rates at the inner/outer surfaces were shown to be proportional to the maximum principal stress and the involved surface.

Pronina [32] employed various corrosion models and proposed a new closed-form analytical solution for plane problems of the mechano-chemical corrosion of an elastic plate with an elliptical hole under uniform remote tension. It was shown that the stress concentration factor is dependent on the relationship between the corrosion kinetics constants and applied stress.

Gutman et al. [33] investigated the stability loss of a thin-walled elastic closed spherical shell under external pressure and internal corrosion. It was illustrated how the critical time of stability loss of the shell can be estimated depending on the upper critical load for static stability loss and the corrosion rate law at different temperatures.

Gutman et al. [34] studied stability loss of a loaded thin-walled spherical shell subjected to internal corrosion. The critical time of the shell stability loss was detected. It was demonstrated that an increase in the safety coefficient for stability yields reduction of the relative durability and that the temperature increase yields an increase in the corrosion rate, and hence a decrease in the vessel lifetime.

Yang et al. [35] analysed the effect of low levels of elastic stress on corrosion behaviour of Q235B steel in an aerated 3.5% NaCl solution by measurements of linear polarization resistance, potentiodynamic polarization characteristics, and electrochemical impedance spectra. New corrosion models were elaborated based on both theoretical and experimental results. Analytical expressions for the structure's lifetime were derived and the effect of corrosion models on lifetime assessment were investigated.

The so far carried out review of the state-of-the-art of modelling and theoretical aspects regarding non-linear vibrations of shells subjected to the mechano-chemical corrosion and coupling of deformation and temperature fields shows that there is a lack of a general theory feasible to fit adequately the phenomena often met in the engineering practice. This motivated us to take a deeper look at the problem of non-linear deformations of geometrically and physically non-linear shallow shells with doubled curvature and static and dynamic loads, taking also the mechano-chemical corrosion wear into account.

The mentioned methodology has been earlier employed to study non-linear dynamics of the structural members including beams, plates, and shells [36–46].

The paper is organized in the following way. A mathematical model of non-linear vibrations of a shallow shell is introduced in Section 2, whereas Section 3 deals with the mathematical model in one-sided corrosion wear conditions. The method of solution, including theorems and their proofs, is reported in Section 4. Section 5 comprises four case studies based on the earlier developed algorithms to solve the problem in a feasible way. The last Section 6 presents concluding remarks.

2. Mathematical model

In this section, the mathematical model of non-linear vibrations of a shallow shell with variable thickness is derived with respect to displacements. It considers the shell subjected to the external normal uniform load. In order to formulate the mathematical model, the following assumptions regarding the shell geometry, material properties, and exploitation conditions are introduced:

(i) transverse shell cross-sections remain planes and are perpendicular to the deformed shell axis (the Kirchhoff–Love hypotheses are satisfied [47]);
(ii) the inertia of rotational shell elements are neglected;
(iii) external forces do not change their directions under the shell deformations;
(iv) the shell planform is significantly bigger than its transverse dimensions;
(v) geometric non-linearity follows the Kármán proposal [48];
(vi) normal stresses can be neglected as their effects are insignificant in comparison with the fundamental stresses, i.e. normal and tangent stresses in the middle shell surface and in the layers parallel to it; this hypothesis can be employed since the studied shell is thin, isotropic and slightly deformed [49,50];
(vii) according to the Dolinskii model, the influence of the corrosion wear is based on the assumption that the corrosion velocity depends linearly on the maximum stresses which are exponentially delayed in time [17];
(viii) the temperature distribution along the shell thickness is arbitrary, i.e. we consider an independent 3D heat transfer PDE;
(ix) the isotropic homogeneous shell with a variable thickness is studied;
(x) dissipative systems are considered.

As it has been mentioned, we introduce the mathematical model of non-linear vibrations of the shallow shell with variable thickness, subjected to the external normal continuous load. The studied shallow shell occupies the region $\Omega = \left\{0 \le x \le a;\ 0 \le y \le b;\ -\frac{h}{2} \le z \le \frac{h}{2} - \delta(x,y)\right\}$ of the R^3 space (Fig. 1).

According to the Kirchhoff hypotheses, displacements u^z, v^z, w^z of an arbitrary point in a certain shell layer parallel to the middle shell layer, with the distance of both layers $z \neq 0$, are governed by the following equations

$$u^z = u(x,y,t) - z\frac{\partial w(x,y,t)}{\partial x},\ v^z = v(x,y,t) - z\frac{\partial w(x,y,t)}{\partial y},\ w^z = w(x,y,t), \quad (1)$$

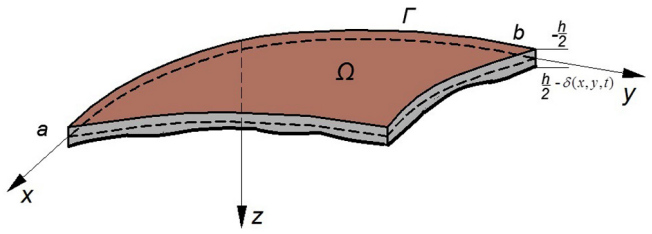

Fig. 1. Scheme of the studied shallow shell.

where $u(x,y,z)$, $v(x,y,z)$ and $w(x,y,z)$ stand for displacements corresponding to the plate's middle surface point in directions x, y, z, respectively.

Full shell deformations ε_{ij}^z, taking into account the geometric Kármán non-linearity, the shell variable thickness, curvature, and thermal deformations, have the following form

$$\begin{aligned}
\varepsilon_{xx}^z &= \frac{\partial u^z}{\partial x} + \frac{1}{2}\left(\frac{\partial w}{\partial x}\right)^2 - k_x w - \frac{1}{2} w \frac{\partial^2 h}{\partial x^2} - \alpha_t T(x,y,z,t) \\
&= \varepsilon_{xx} + z\chi_{xx} + \varepsilon_{xx}^t, \\
\varepsilon_{yy}^z &= \frac{\partial v^z}{\partial y} + \frac{1}{2}\left(\frac{\partial w}{\partial y}\right)^2 - k_y w - \frac{1}{2} w \frac{\partial^2 h}{\partial y^2} - \alpha_t T(x,y,z,t) \\
&= \varepsilon_{yy} + z\chi_{yy} + \varepsilon_{yy}^t, \\
\varepsilon_{xy}^z &= \frac{1}{2}\left(\frac{\partial u^z}{\partial y} + \frac{\partial v^z}{\partial x}\right) + \frac{\partial w}{\partial x}\frac{\partial w}{\partial y} - \frac{1}{2} w \frac{\partial^2 h}{\partial x \partial y} \\
&= \varepsilon_{xy} + z\chi_{xy}.
\end{aligned} \tag{2}$$

Here: ε_{ij} — tangential deformations; χ_{ij} — bending deformations; $\varepsilon_{xx}^t, x \longleftrightarrow y$ — temperature deformations; $k_x = \frac{1}{R_x}$, $k_y = \frac{1}{R_y}$ — geometric shell parameters; R_x, R_y — curvatures of the shell surface; $h = h(x,y)$ — function of the changes in the shell thickness; α_t — coefficient of heat extension of the shell material; $T(x,y,z,t)$ — function of the temperature field.

The relations between stresses and deformations have the following forms

$$\sigma_{xx} = \frac{E}{1-\nu^2}\left(\varepsilon_{xx}^z - \nu\varepsilon_{yy}^z\right), \qquad \sigma_{xy} = \sigma_{yx} = \frac{E}{2(1+\nu)}\varepsilon_{xy}^z, \tag{3}$$

where E, ν stand for Young's modulus and Poisson's ratio, respectively.

Equations of motion as well as boundary and initial conditions of the shell are yielded by Hamilton's principle. Namely, two neighbourhood motions of the system of material points from their initial state at the time instant t_0 to the terminal state at the time instant t_1 are compared. In the case of the real (true) motion, the following relation holds

$$\int_{t_0}^{t_1} (\delta K - \delta \Pi + \delta W) dt = 0, \tag{4}$$

where: K — shell kinetic energy; Π — potential shell energy; $\delta W = \delta W_q + \delta W_\varepsilon$ — variations of the external W_q and damping W_ε forces, and

$$\begin{aligned}
K &= \frac{1}{2}\frac{\gamma}{g}\int_\Omega \left[\left(\frac{\partial u^z}{\partial t}\right)^2 + \left(\frac{\partial v^z}{\partial t}\right)^2 + \left(\frac{\partial w^z}{\partial t}\right)^2\right] dv, \\
\Pi &= \frac{1}{2}\int_\Omega \left[\sigma_{xx}\varepsilon_{xx}^z + \sigma_{yy}\varepsilon_{yy}^z + 2\sigma_{xy}\varepsilon_{xy}^z\right] dv, \\
\delta W_\varepsilon &= \int_\Omega \left[\varepsilon\frac{\gamma}{g}\frac{\partial w}{\partial t}\delta w\right] dv, \\
\delta W_q &= \int_0^a \int_0^b q(x,y,t)\,\delta w dx dy.
\end{aligned} \tag{5}$$

Here, γ is a specific weight of the shell material; g denotes the gravity of Earth; ε is the external damping coefficient; $q(x,y,t)$ is the external normal load; $\int_\Omega (.)\,dv = \int_0^a \int_0^b \int_{-\frac{h(x,y)}{2}}^{\frac{h(x,y)}{2}-\delta(x,y)} (.)\,dz dy dx$, and $\delta(x,y)$ describes the function of the height of corrosion material damage.

Substituting (5) into (1)–(3), taking into account (4), carrying out variations with respect to the variables u, v, w, carrying out the integrations by parts, and comparing the expressions standing by δu, δv, and δw to zero, one can obtain the following equations of motion

$$\begin{aligned}
&\frac{\partial}{\partial x}\left(N_{xx}\frac{\partial w}{\partial x}\right) + \frac{1}{2}N_{xx}\frac{\partial^2 h}{\partial x^2} + k_x N_{xx} + \frac{\partial^2 M_x}{\partial x^2} + \frac{\partial}{\partial y}\left(N_{yy}\frac{\partial w}{\partial y}\right) \\
&+\frac{1}{2}N_{yy}\frac{\partial^2 h}{\partial y^2} + k_y N_{yy} + \frac{\partial^2 M_y}{\partial y^2} - \\
&+N_{xy}\frac{\partial^2 h}{\partial x \partial y} + \frac{\partial N_{xy}}{\partial x}\frac{\partial w}{\partial y} + 2N_{xy}\frac{\partial^2 w}{\partial x \partial y} + \frac{\partial N_{xy}}{\partial y}\frac{\partial w}{\partial x} + 2\frac{\partial^2 H}{\partial x \partial y} \\
&-\frac{\gamma(h-\delta)}{g}\frac{\partial^2 w}{\partial t^2} \\
&+\frac{\delta(h-\delta)\gamma}{g}\left(\frac{\partial^3 u}{\partial t^2 \partial x} + \frac{\partial^3 v}{\partial t^2 \partial y}\right) + \frac{\gamma\left(h^3 - 3h^2\delta + 6h\delta^2 - 4\delta^3\right)}{6g} \\
&\times\left(\frac{\partial^4 w}{\partial t^2 \partial x^2} + \frac{\partial^4 w}{\partial t^2 \partial y^2}\right) + \varepsilon\frac{\gamma(h-\delta)}{g}\frac{\partial w}{\partial t} + 2q = 0, \\
&\frac{\partial N_{xx}}{\partial x} + \frac{1}{2}\frac{\partial N_{xy}}{\partial y} - \frac{\gamma(h-\delta)}{g}\frac{\partial^2 u}{\partial t^2} + \frac{\delta(\delta-h)\gamma}{g}\frac{\partial^3 w}{\partial t^2 \partial x} = 0, \\
&\frac{\partial N_{yy}}{\partial y} + \frac{1}{2}\frac{\partial N_{xy}}{\partial x} - \frac{\gamma(h-\delta)}{g}\frac{\partial^2 v}{\partial t^2} + \frac{\delta(\delta-h)\gamma}{g}\frac{\partial^3 w}{\partial t^2 \partial y} = 0,
\end{aligned} \tag{6}$$

as well as the following boundary conditions

$$\begin{aligned}
&\delta w = 0 \quad or \quad \left\{N_{xx}\frac{\partial w}{\partial x} + 2N_{xy}\frac{\partial w}{\partial y}\right\}_{n_x} + \left\{N_{yy}\frac{\partial w}{\partial y} + 2N_{xy}\frac{\partial w}{\partial x}\right\}_{n_y} = 0, \\
&\frac{\partial \delta w}{\partial x} = 0 \quad or \quad \{M_{xx}\}_{n_x} + \{2H\}_{n_y} = 0, \\
&\frac{\partial \delta w}{\partial y} = 0 \quad or \quad \{2H\}_{n_x} + \{M_{yy}\}_{n_y} = 0, \\
&\delta u = 0 \quad or \quad \{N_{xx}\}_{n_x} + \{N_{xy}\}_{n_y} = 0, \\
&\delta v = 0 \quad or \quad \{N_{xy}\}_{n_x} + \{N_{yy}\}_{n_y} = 0.
\end{aligned}$$

Expressions for the forces and moments, taking the account of the temperature field are as follows

$$\begin{aligned}
N_{xx} &= \int_{-h(x,y)/2}^{h(x,y)/2-\delta(x,y)} \sigma_{yy} dz = C_{0,0}^1 \left\{\left[\frac{\partial u}{\partial x} + \frac{1}{2}\left(\frac{\partial w}{\partial x}\right)^2 - k_x w - \frac{1}{2} w \frac{\partial^2 h}{\partial x^2}\right]\right. \\
&\left. - \nu\left[\frac{\partial v}{\partial y} + \frac{1}{2}\left(\frac{\partial w}{\partial y}\right)^2 - k_y w - \frac{1}{2} w \frac{\partial^2 h}{\partial y^2}\right]\right\} - N_t \\
&+C_{1,0}^1\left(-\frac{\partial^2 w}{\partial x^2} + \nu\frac{\partial^2 w}{\partial y^2}\right),
\end{aligned}$$

$$\begin{aligned}
N_{yy} &= \int_{-h(x,y)/2}^{h(x,y)/2-\delta(x,y)} \sigma_{yy} dz = C_{0,0}^1 \left\{\left[\frac{\partial v}{\partial y} + \frac{1}{2}\left(\frac{\partial w}{\partial y}\right)^2 - k_y w - \frac{1}{2} w \frac{\partial^2 h}{\partial y^2}\right]\right. \\
&\left. - \nu\left[\frac{\partial u}{\partial x} + \frac{1}{2}\left(\frac{\partial w}{\partial x}\right)^2 - k_x w - \frac{1}{2} w \frac{\partial^2 h}{\partial x^2}\right]\right\} - N_t + C_{1,0}^1\left(-\frac{\partial^2 w}{\partial y^2} + \nu\frac{\partial^2 w}{\partial x^2}\right), \\
N_{xy} &= \int_{-h(x,y)/2}^{h(x,y)/2-\delta(x,y)} \sigma_{xy} dz = \frac{1}{2}C_{0,0}^2\left[\frac{\partial u}{\partial y} + \frac{\partial v}{\partial x} + \frac{\partial w}{\partial x}\frac{\partial w}{\partial y} - w\frac{\partial^2 h}{\partial x \partial y}\right] \\
&- \frac{1}{2}C_{0,0}^2\frac{\partial^2 w}{\partial x \partial y},
\end{aligned}$$

$$\begin{aligned}
M_{xx} &= \int_{-h(x,y)/2}^{h(x,y)/2-\delta(x,y)} \sigma_{xx} z dz \\
&= C_{1,0}\left\{\left[\frac{\partial u}{\partial x} + \frac{1}{2}\left(\frac{\partial w}{\partial x}\right)^2 - k_x w - \frac{1}{2} w \frac{\partial^2 h}{\partial x^2}\right]\right. \\
&\left. - \nu\left[\frac{\partial v}{\partial y} + \frac{1}{2}\left(\frac{\partial w}{\partial y}\right)^2 - k_y w - \frac{1}{2} w \frac{\partial^2 h}{\partial y^2}\right]\right\} - M_t \\
&+C_{2,0}\left\{-\frac{\partial^2 w}{\partial x^2} + \nu\frac{\partial^2 w}{\partial y^2}\right\},
\end{aligned}$$

$$
\begin{aligned}
M_{yy} &= \int_{-h(x,y)/2}^{h(x,y)/2-\delta(x,y)} \sigma_{yy} z dz \\
&= C_{1,0}^1 \left\{ \left[\frac{\partial v}{\partial y} + \frac{1}{2}\left(\frac{\partial w}{\partial y}\right)^2 - k_y w - \frac{1}{2} w \frac{\partial^2 h}{\partial y^2} \right] \right. \\
&\left. - \nu \left[\frac{\partial u}{\partial x} + \frac{1}{2}\left(\frac{\partial w}{\partial x}\right)^2 - k_x w - \frac{1}{2} w \frac{\partial^2 h}{\partial x^2} \right] \right\} - M_t \\
&+ C_{2,0}^1 \left\{ -\frac{\partial^2 w}{\partial x^2} + \nu \frac{\partial^2 w}{\partial x^2} \right\},
\end{aligned} \tag{7}
$$

$$
\begin{aligned}
H &= \int_{-h(x,y)/2}^{h(x,y)/2-\delta(x,y)} \sigma_{xy} z dz = \frac{1}{2} C_{1,0}^2 \left[\frac{\partial u}{\partial y} + \frac{\partial v}{\partial x} + \frac{\partial w}{\partial x}\frac{\partial w}{\partial y} - w \frac{\partial^2 h}{\partial x \partial y} \right] \\
&- C_{2,0}^2 \frac{\partial^2 w}{\partial x \partial y}.
\end{aligned}
$$

where: $C_{i,j}^1 = \frac{E}{1-\nu^2} \int_{-h(x,y)/2}^{h(x,y)/2-\delta(x,y)} z^i dz$, $C_{i,j}^2 = \frac{E}{2(1+\nu)} \int_{-h(x,y)/2}^{h(x,y)/2-\delta(x,y)} z^i dz$ are the stiffnesses, and $N_t = \frac{E}{1+\nu} \int_{-h(x,y)/2}^{h(x,y)/2-\delta(x,y)} \alpha_t T(x,y,z,t) dz$, $M_t = \frac{E}{1+\nu} \int_{-h(x,y)/2}^{h(x,y)/2-\delta(x,y)} \alpha_t T(x,y,z,t) z dz$ stand for thermal forces and moments. The corrosion wear, according to Dolinskii [17], takes the form

$$
\frac{\partial \eta}{\partial t} = \varphi(t)(1 + k\sigma_i), \tag{8}
$$

where $\varphi(t) = \frac{a+b\exp(\beta t-1)}{\exp(\beta t)}$, and σ_i stand for the stresses intensities, whereas a, b are the coefficients obtained experimentally.

As it has been already mentioned, there are no *a priori* constraints imposed on the temperature distribution along the shell thickness, and hence the following 3D heat transfer PDE taking into account the coupling of deformation and temperature fields holds

$$
\frac{C_0}{T_0}\frac{\partial T}{\partial t} - \frac{\lambda}{T_0}\left(\frac{\partial^2 T}{\partial x^2} + \frac{\partial^2 T}{\partial x^2} + \frac{\partial^2 T}{\partial z^2}\right) = \frac{E\,\alpha_t}{1-\nu}\left(\frac{\partial \varepsilon_{xx}}{\partial t} + \frac{\partial \varepsilon_{yy}}{\partial t}\right), \tag{9}
$$

where C_0 is the specific heat capacity of the shell material and T_0 stands for the shell temperature in its undeformed state.

Therefore, the following full system of PDEs governing the behaviour of the shell with a variable thickness and subjected to the action of coupled temperature and deformation fields as well as one-sided mechanical corrosion wear is obtained

$$
\begin{aligned}
&\frac{\partial}{\partial x}\left(N_{xx}\frac{\partial w}{\partial x}\right) + \frac{1}{2}N_{xx}\frac{\partial^2 h}{\partial x^2} + k_x N_{xx} + \frac{\partial^2 M_x}{\partial x^2} + \frac{\partial}{\partial y}\left(N_{yy}\frac{\partial w}{\partial y}\right) \\
&+\frac{1}{2}N_{yy}\frac{\partial^2 h}{\partial y^2} + k_y N_{yy} + \frac{\partial^2 M_y}{\partial y^2} - N_{xy}\frac{\partial^2 h}{\partial x \partial y} + \frac{\partial N_{xy}}{\partial x}\frac{\partial w}{\partial y} \\
&+2N_{xy}\frac{\partial^2 w}{\partial x \partial y} + \frac{\partial N_{xy}}{\partial y}\frac{\partial w}{\partial x} + 2\frac{\partial^2 H}{\partial x \partial y} - \frac{\gamma(h-\delta)}{g}\frac{\partial^2 w}{\partial t^2} \\
&+\frac{\delta(h-\delta)\gamma}{g}\left(\frac{\partial^3 u}{\partial t^2 \partial x} + \frac{\partial^3 v}{\partial t^2 \partial y}\right) \\
&+\frac{\gamma\left(h^3 - 3h^2\delta + 6h\delta^2 - 4\delta^3\right)}{6g}\left(\frac{\partial^4 w}{\partial t^2 \partial x^2} + \frac{\partial^4 w}{\partial t^2 \partial y^2}\right) \\
&+\varepsilon\frac{\gamma(h-\delta)}{g}\frac{\partial w}{\partial t} + 2q = 0, \\
&\frac{\partial N_{xx}}{\partial x} + \frac{1}{2}\frac{\partial N_{xy}}{\partial y} - \frac{\gamma(h-\delta)}{g}\frac{\partial^2 u}{\partial t^2} + \frac{\delta(\delta-h)\gamma}{g}\frac{\partial^3 w}{\partial t^2 \partial x} = 0, \\
&\frac{\partial N_{yy}}{\partial y} + \frac{1}{2}\frac{\partial N_{xy}}{\partial x} - \frac{\gamma(h-\delta)}{g}\frac{\partial^2 v}{\partial t^2} + \frac{\delta(\delta-h)\gamma}{g}\frac{\partial^3 w}{\partial t^2 \partial y} = 0, \\
&\frac{\partial \delta}{\partial t} = \varphi(t)(1 + k\sigma_i), \\
&\frac{C_0}{T_0}\frac{\partial T}{\partial t} - \frac{\lambda}{T_0}\left(\frac{\partial^2 T}{\partial x^2} + \frac{\partial^2 T}{\partial x^2} + \frac{\partial^2 T}{\partial z^2}\right) = \frac{E\,\alpha_t}{1-\nu}\left(\frac{\partial \varepsilon_{xx}^z}{\partial t} + \frac{\partial \varepsilon_{yy}^z}{\partial t}\right).
\end{aligned} \tag{10}
$$

The following initial conditions are supplemented to the governing equation (10):

$$
\begin{aligned}
&w(x,y,t) = \varphi_{30}(x,y); v(x,y,t) = \varphi_{20}(x,y); u(x,y,t) = \varphi_{10}(x,y), \\
&T(x,y,z,t) = \varphi_4(x,y,z); \delta(x,y,t) = \varphi_5(x,y), \\
&\frac{\partial w(x,y,t)}{\partial t} = \psi_{30}(x,y), \quad \frac{\partial u(x,y,t)}{\partial t} = \psi_{20}(x,y), \\
&\frac{\partial u(x,y,t)}{\partial t} = \psi_{10}(x,y), \quad t = 0.
\end{aligned} \tag{11}
$$

The boundary conditions depend on the loading conditions and the type of clamping of the shell edges. Here, $\varphi_{i0}(x)$, $\psi_{i0}(x)$, $\varphi_4(x,z)$, $\varphi_5(x)$ stand for the known functions defining the initial shell state. Observe that the system of equations describing the motion of the shell element (6) includes the fourth-order derivatives with respect to coordinates, which plays a key role while proving the existence of a solution and convergence of different numerical methods used.

3. Mathematical model in conditions of one-sided corrosion wear

We investigate stability of a flexible shell under the one-sided corrosion wear. We assume that one side of the shell is embedded in an aggressive environment, whereas the remaining side is isolated. The shell is subjected to transverse and longitudinal compression. Although the shell material is assumed to be isotropic but non-homogeneous, contrarily to what was presented in Section 1. Observe that $\varepsilon^z = \frac{1}{E}\left(\sigma_x - \nu\sigma_y\right)$ coincides with Hooke's law for the plane stress state only at the first glance. Here E and ν are complex functions $E = E(x,y,z,\varepsilon_0,\varepsilon_i)$, $\nu = \nu(x,y,z,\varepsilon_0,\varepsilon_i)$, in a given point instead of the fixed Young's modulus and Poisson's ratio defined in the classical linear case. A similar approach has been used by Birger, who employed the method of variable parameters of elasticity to investigate elastic and elastic–plastic problems. While solving specific problems, there is no need to know the functions E and ν. Here we discuss only their widely met variants: $E = E(x,y,z)$, $\nu = \nu(x,y,z)$ and $E = E(\varepsilon_0,\varepsilon_i)$, $\nu = \nu(\varepsilon_0,\varepsilon_i)$, corresponding to a nonhomogeneous, physically linear material and a homogeneous, physically nonlinear material, respectively. The values of the mentioned functions change with the change in the deformable state in the given material point. Therefore, a physically nonlinear body can be considered as a body whose nonhomogeneity depends on its deformable state nonlinearly, although its properties are physically linear. Physical parameters E and G are unique functions with respect to the given point and its associated deformable state. This plays an important role when it comes to using nonlinear theories of elastic (inversed) deformations and small elastic–plastic deformations without the lack of relaxation. The deformed state of a material point is characterized by the volume deformation ε_0 and the deformation intensity ε_i. In a standard problem formulation, the hypotheses on straight normals are exhibited by preserving the length of a normal element, which corresponds to the neglection of deformations ε_{zz} in comparison to unity (1). However, in the expressions ε_0 and ε_i, this vector appears together with other components of the same order and we cannot neglect the terms ε_{zz}. In order to estimate ε_{zz}, while computing ε_0 and ε_i, we employ the following condition of the plane stress state: $\varepsilon_{zz} = 0$. Here we do not consider the thermal deformations.

Taking into account the physical non-linearity, forces $N_{xx} = \int_{-h(x,y)/2}^{h(x,y)/2-\delta(x,y)} \sigma_{xx} dz$, $x \leftrightarrow y$ and moments $M_{xx} = \int_{-h(x,y)/2}^{h(x,y)/2-\delta(x,y)} z\sigma_{xx} dz$, $H = \int_{-h(x,y)/2}^{h(x,y)/2-\delta(x,y)} z\sigma_{xy} dz$, $x \leftrightarrow y$, can be recast to the following explicit forms:

$$
\begin{aligned}
N_{xx} &= C_{00}\varepsilon_{xx} + C_{01}\varepsilon_{yy} + C_{10}\chi_{xx} + C_{11}\chi_{yy}, N_{yy} = C_{01}\varepsilon_{xx} + C_{00}\varepsilon_{yy} \\
&\quad + C_{11}\chi_{xx} + C_{10}\chi_{yy}, \\
N_{xy} &= \frac{1}{2}(E_{00}\varepsilon_{xy} + E_{10}\chi_{xy}), M_{xx} = C_{10}\varepsilon_{xx} + C_{11}\varepsilon_{yy} + C_{20}\chi_{xx} + C_{21}\chi_{yy}, \\
M_{yy} &= C_{11}\varepsilon_{xx} + C_{10}\varepsilon_{yy} + C_{21}\chi_{xx} + C_{20}\chi_{yy}, H = \frac{1}{2}(E_{10}\varepsilon_{xy} + E_{20}\chi_{xy}),
\end{aligned} \tag{12}
$$

where the respective stiffnesses are as follows

$$
C_{ij} = \frac{1}{2}\left[E_{ij} + (-1)^j E_{i0}\right], E_{ij} = \int_{-h(x,y)/2}^{h(x,y)/2-\delta(x,y)} \frac{E z^i}{1 + (-1)^j \nu} dz. \tag{13}
$$

We consider a class of problems governed by PDEs in the mixed form and we employ the following stress (Airy's) function

$$
N_{xx} = \frac{\partial^2 F}{\partial y^2} - P_1, N_{yy} = \frac{\partial^2 F}{\partial y^2} - P_2, N_{xy} = -\frac{\partial^2 F}{\partial x \partial y}, \tag{14}
$$

where P_x, P_y stand for the longitudinal load.

The potential energy of shell deformation (5) consists of the potential energy of bending and the potential energy of the middle shell surface $\Pi = \Pi_b + \Pi_s$. Variation of the potential energy of the middle shell surface has the following form:

$$\delta\Pi_s = \delta \iint_S \left(N_{xx}\varepsilon_{xx} + N_{yy}\varepsilon_{yy} + N_{xy}\varepsilon_{xy}\right) dS + \iint_S \left(Q_x\delta\varepsilon_{xz} + Q_y\delta\varepsilon_{yz}\right) dS, \tag{15}$$

where Q_x, Q_y are the transverse forces per unit length. In order to get equations in the mixed form through the stress function and displacement along the z coordinate, we recast $\delta\Pi_s$ to the following, more feasible form

$$\delta\Pi_s = \delta \iint_S \left(N_{xx}\varepsilon_{xx} + N_{yy}\varepsilon_{yy} + N_{xy}\varepsilon_{xy} + Q_x\delta\varepsilon_{xz} + Q_y\delta\varepsilon_{yz}\right) dS - \iint_S \left(\varepsilon_{xx}\delta N_{xx} + \varepsilon_{yy}\delta N_{yy} + \varepsilon_{xy}\delta N_{xy}\right) dS. \tag{16}$$

Relation (16) contains variations of stresses with respect to the shell middle surface. Observe that, formally, relations (15) and (16) are equivalent, but the employment of the formula (16) enables one to introduce the variation with respect to the mixed type equation, where the variation takes place along the displacement w and the stress function F.

As a result, we obtain differential equations of the equilibrium and deformation continuity of the following form

$$\begin{aligned}
&\frac{\partial^2}{\partial x^2}\left(A_2\frac{\partial^2 F}{\partial y^2} + \frac{A_1}{\lambda^2}\frac{\partial^2 F}{\partial x^2}\right) + \frac{\partial^2}{\partial y^2}\left(A_1\lambda^2\frac{\partial^2 F}{\partial y^2} + A_2\frac{\partial^2 F}{\partial x^2}\right)\\
&+2\frac{\partial^2}{\partial x\partial y}\left(\left(A_1 - A_2\right)\frac{\partial^2 F}{\partial x\partial y}\right) - \frac{\partial^2}{\partial y^2}\left(A_1P_1 + A_2P_2\right)\\
&-\frac{\partial^2}{\partial x^2}\left(A_2P_1 + A_1P_2\right) = -\frac{\partial^2}{\partial x^2}\left(\frac{B_{11}}{\lambda^2}\frac{\partial^2 w}{\partial x^2} + B_{10}\frac{\partial^2 w}{\partial y^2}\right)\\
&-\frac{\partial^2}{\partial y^2}\left(B_{10}\frac{\partial^2 w}{\partial x^2} + \lambda^2 B_{11}\frac{\partial^2 w}{\partial y^2}\right)\\
&-2\frac{\partial^2}{\partial x\partial y}\left(\left(B_{11} - B_{10}\right)\frac{\partial^2 w}{\partial x\partial y}\right) - \frac{1}{2}L\left(w + \frac{h}{2}, w\right) - \nabla_k^2 w,
\end{aligned} \tag{17}$$

$$\begin{aligned}
&\frac{\partial^2}{\partial x^2}\left(\frac{B_{11}}{\lambda^2}\frac{\partial^2 w}{\partial x^2} + B_{10}\frac{\partial^2 w}{\partial y^2}\right) + \frac{\partial^2}{\partial y^2}\left(B_{10}\frac{\partial^2 w}{\partial x^2} + \lambda^2 B_{11}\frac{\partial^2 F}{\partial y^2}\right)\\
&+2\frac{\partial^2}{\partial x\partial y}\left(\left(B_{11} - B_{10}\right)\frac{\partial^2 w}{\partial x\partial y}\right) + \frac{1}{2}L\left(w + \frac{h}{2}, F\right)\\
&= -\frac{\partial^2}{\partial y^2}\left(B_{10}\frac{\partial^2 F}{\partial y^2} + \frac{B_{11}}{\lambda^2}\frac{\partial^2 F}{\partial x^2}\right) - \frac{\partial^2}{\partial y^2}\left(\lambda^2 B_{11}\frac{\partial^2 F}{\partial y^2} + B_{10}\frac{\partial^2 F}{\partial x^2}\right)\\
&-2\frac{\partial^2}{\partial x\partial y}\left(\left(B_{11} - B_{10}\right)\frac{\partial^2 F}{\partial x\partial y}\right)\\
&-\frac{\partial^2}{\partial x^2}\left(B_{10}P_1 + B_{11}P_2\right) - \frac{\partial^2}{\partial y^2}\left(B_{11}P_1 + B_{10}P_2\right)\\
&-P_1\left(\frac{\partial^2 w}{\partial y^2} + \frac{\partial^2 h}{\partial x^2}\right) - P_2\left(\frac{\partial^2 w}{\partial x^2} + \frac{\partial^2 h}{\partial y^2}\right) - q + \nabla_k^2 F.
\end{aligned} \tag{18}$$

In the above equation: $A_j = \frac{1}{2}\left[\frac{1}{D_{01}} + (-1)^{j+1}\frac{1}{D_{00}}\right]$, $B_{ik} = \frac{1}{2}\left[\frac{D_{i1}}{D_{01}} + (-1)^k\frac{D_{i0}}{D_{00}}\right]$, $\nabla_k^2 = k_x\frac{\partial^2}{\partial x^2} + k_y\frac{\partial^2}{\partial y^2}$, $B_{ik}^* = \frac{1}{2}\left[\frac{D_{i1}^2}{D_{01}} + (-1)^{k+1}\frac{D_{i0}^2}{D_{00}}(-1)^k D_{20} - D_{21}\right]$, $D_{ij} = \int_{-h(x,y)/2}^{h(x,y)/2-\delta(x,y)} \frac{Ez^i}{1+(-1)^j\upsilon^2}dz$.

Eqs. (17)–(18) are recast to their counterpart forms through the following relations:

$$\bar{x} = \frac{x}{a}, \bar{y} = \frac{y}{b}, \bar{z} = \frac{z}{h_0}, \bar{h} = \frac{h}{h_0}, \lambda = \frac{a}{b}, \lambda_1 = \frac{a}{h_0}, \bar{t} = \frac{t}{t_0}, \bar{F} = \frac{F}{Eh_0^3},$$

$$\bar{q} = \frac{qa^2b^2}{G_0h_0^4}, e_s = e_{is}\lambda_1^2, e_i = e_i\lambda_1^2,$$

$$\sigma_s = \sigma_{is}G_0^{-1}\lambda_1^2, \bar{E} = EG_0^{-1}, \bar{G_1} = G_1G_0^{-1}, \bar{B_{ij}} = B_{ij}h_0^{-1}, \bar{A_i} = A_iG_0^{-1}h_0^{-1},$$

$$\bar{E_{ij}} = \frac{E_{ij}}{G_0h_0^{i+1}}, \bar{\varepsilon_{ij}} = \frac{\varepsilon_{ij}}{\lambda_1^2},$$

$$\bar{\sigma_{ij}} = \sigma_{ij}G_0^{-1}\lambda_1^2, \bar{e_{ij}} = e_{ij}\lambda_1^2, \bar{P_i} = P_iG_0^{-1}h_0^{-3}, \bar{B}_{03}^2 = B_{03}^2G_0^{-1}\frac{(\mu-1)}{8\pi\mu}h_0^{-2}.$$

In addition, PDEs (17)–(18) are supplemented by initial and boundary conditions corresponding to loading and damping conditions. It should be emphasized that the obtained system of resolving PDEs can be viewed as a modification of the Kármán equations for the problems of one-sided corrosion wear of the shallow shell.

The system of Eqs. (17)–(18) includes geometric and physical non-linearity which essentially complicate the process of finding reliable solutions. In what follows, to simplify the problem, we employ the iterational procedure for the Kármán equations [48]. Below, we prove convergence of the above-mentioned procedure.

4. Method of solution

The system of Eqs. (17), (18), without physical non-linearity and corrosion wear, takes the following form

$$\begin{cases} k\,\Delta^2 w - L(w,F) - q = 0,\\ \Delta^2 F + \frac{1}{2}L(w,w) = 0. \end{cases} \tag{19}$$

In (19), $L(w,F)$ and $L(w,w)$ stand for the well-known non-linear differential operators.

Boundary conditions take the form

$$w|_\Gamma = \left.\frac{\partial^2 w}{\partial n^2}\right|_\Gamma = F|_\Gamma = \left.\frac{\partial^2 F}{\partial n^2}\right|_\Gamma = 0, \tag{20}$$

$$w|_\Gamma = \left.\frac{\partial^2 w}{\partial n^2}\right|_\Gamma = F|_\Gamma = \left.\frac{\partial F}{\partial n}\right|_\Gamma = 0, \tag{21}$$

where n is normal to Γ.

We leave only bi-harmonic operators on the left-hand side of the latter PDEs and shift the non-linear terms to the right-hand side. Assuming that the function on the right-hand side can be computed taking into account the previous computational step and assuming that the equations can be solved successively, the following iterational procedure is used:

$$\begin{cases} k\,\Delta^2 w^{(k)} = L\left(w^{(k-1)}, F^{(k-1)}\right) + q,\\ \Delta^2 F^{(k)} = -\frac{1}{2}L\left(w^{(k)}, w^{(k)}\right), \quad \{x,y\} \in \Omega. \end{cases} \tag{22}$$

In the first step of the iterational procedure, the following bi-harmonic equation is solved for the given load $q(x,y)$:

$$\Delta^2 w^{(1)}(x,y) = q(x,y).$$

The obtained value $w^{(1)}(x,y)$ is substituted in the right-hand side of the second equation of the system (20) and, as a result, we obtain a bi-harmonic equation with respect to $F^{(1)}(x,y)$ with the known right-hand side. The found value of the stress function is then substituted in the first equation of the studied system. The so far described process is terminated when the assumed accuracy is obtained.

Observe that as a result of the application of the mentioned iterational procedure, the system of equations of the Germain–Lagrange type is obtained.

It should be mentioned that the development of the proof of existence of a solution to the corresponding boundary value problems is one of the most important and difficult processes while constructing theories of beams, plates and shells [51–54].

Proof of convergence of the developed iterational procedure (the given proof is original).

We denote by $H^2(\Omega)$ the Sobolev space of functions $\xi = \{w, F\}$ such that $\xi \in L^2(\Omega)$, $\frac{\partial\xi}{\partial x_i} \in L^2(\Omega)$, $\frac{\partial^2\xi}{\partial x_i\partial x_j} \in L^2(\Omega)$; $i,j = 1,2$, where $L^2(\Omega)$ stand for the functions summed with the square in Ω.

By $H_0^2(\Omega)$ we denote the closure of the function $D(\Omega)$ (the space of the function of the class C^∞ in Ω, having a compact carrier in Ω) in the norm $H^2(\Omega)$:

$$H_0^2(\Omega) = \overline{D(\Omega)}^{H^2(\Omega)} = \left\{\xi \in H^2(\Omega)\middle|\ \xi|_\Gamma = \left.\frac{\partial\xi}{\partial n}\right|_\Gamma = 0\right\}.$$

Since the space Ω is bounded and its boundary Γ is sufficiently regular, the map $\xi \to \|\Delta\xi\|_{0,\Omega}$ defines the norm in $H_0^2(\Omega)$, which is equivalent to the norm induced in the space $H^2(\Omega)$.

Let us assume that $q \in H^{-2}(\Omega)$ ($H^{-2}(\Omega)$ means conjugated to $H^2(\Omega)$). It is known [55] that in this case, the problem (18), (20)–(21) has a solution (although not necessarily unique).

New variational formulation of the problem

Let us denote by $(\cdot\,,\,\cdot)$ a scalar product in $L^2(\Omega)$:$(\xi,\eta) = \int_\Omega \xi\,\eta\; d\Omega$, an by $\beta(w,F,\mu)$ a three-linear form defined on $\left(H_0^2(\Omega)\right)^3$:

$$\beta(w,F,\mu) = (\Delta F, \Delta\mu) + \frac{1}{2}(L(w,w),\mu)\,. \tag{23}$$

Let us introduce a set

$$M = \left\{w, F \in H_0^2(\Omega) \mid \ \forall\mu \in H_0^2(\Omega),\ \ \beta(w,F,\mu) = 0\right\}, \tag{24}$$

and a square function $J(w,F) : M \to R$

$$J(w,F) = \frac{1}{2}\|\Delta w\|_{0,\Omega}^2 + \frac{1}{2}\|\Delta F\|_{0,\Omega}^2 - (q,w)\,. \tag{25}$$

Theorem 1. *The problem of minimization of (25) on the set (24) has at least one solution.*

Proof. Let $\{w_n, F_n\} \in M$ stand for the minimization sequence, i.e.

$$J(w_n,F_n) \to \inf_{\{w,F\}\in M} J(w,F)\,, \tag{26}$$

which exists since J stands for the square functional.

For arbitrary $w, F \in H_0^2(\Omega)$, the following inequality holds

$$J(w,F) \geq c_1\|w\|_{2,\Omega}^2 + c_2\|F\|_{2,\Omega}^2 - c_3.\|w\|_{2,\Omega}\,,$$

where $\|\cdot\|_{2,\Omega}$ is a norm in $H^2(\Omega)$, and c_i are certain positive constants. It follows from (26) that

$$c_1\|w_n\|_{2,\Omega}^2 + c_2\|F_n\|_{2,\Omega}^2 - c_3\|w_n\|_{2,\Omega} \leq J(w_n,F_n) \leq J(w_0,F_0) = A,$$

where w_0, F_0 are arbitrarily chosen functions (initial approximation).

Hence, we get

$$c_1\left(\|w_n\|_{2,\Omega}^2 - \frac{c_3}{2c_1}\right)^2 + c_2\|F_n\|_{2,\Omega}^2 \leq A + \frac{c_3^2}{4c_1},\quad \|w_n\|_{2,\Omega} \leq c_4,$$
$$\|F_n\|_{2,\Omega} \leq c_5.$$

Therefore, the series $\{w_n, F_n\}$ is bounded in $\left(H_0^2(\Omega)\right)^2$. Consequently, one can take a subseries $\{w_k, F_k\}$ such that $w_k \to \tilde{w}$, $F_k \to \tilde{F}$ is weak in $H_0^2(\Omega)$. Since the embedding $H_0^2(\Omega) \to L^2(\Omega)$ is compact, $w_k \to \tilde{w}$, $F_k \to \tilde{F}$ is strong in $L^2(\Omega)$.

We show that the limit $\{\tilde{w}, \tilde{F}\}$ of the minimizing series belongs to M, i.e. that $\beta(\tilde{w},\tilde{F},\mu) = 0, \quad \forall\mu \in H_0^2(\Omega)$.

Since $(L(w_k,w_k),\mu) = (L(w_k,\mu),w_k) \quad \forall\mu \in H_0^2(\Omega)$ and $L(w_k,\mu) \to L(\tilde{w},\mu)$ are weak in $H_0^2(\Omega)$, taking into account that $w_k \to \tilde{w}$ is strong in $L^2(\Omega)$, one gets: $(L(w_k,w_k),\mu) = (L(\tilde{w},\tilde{w}),\mu)$ and, consequently, $\beta(\tilde{w},\tilde{F},\mu) = 0 \quad \forall\mu \in H_0^2(\Omega)$. This implies

$$\{\tilde{w},\tilde{F}\} \in M\,. \tag{27}$$

However, $J(w,F)$ is semi-continuous from below in a weak topology on $\left(H^2(\Omega)\right)^2$, and hence the following inequality holds $\lim_{k\to\infty} J(w_k,F_k) \geq J(\tilde{w},\tilde{F})$. Then, it follows from (26) and (27) that $J(\tilde{w},\tilde{F}) \leq \inf_{(w,F)\in M} J(w,F)$. Therefore, the following equality holds $J(\tilde{w},\tilde{F}) = \inf_{(w,F)\in M} J(w,F)$, which means that $\{\tilde{w},\tilde{F}\} \in M$ stands for the solution to the problem of minimization. ■

Therefore, it has been proved that there is at least one solution in the case of minimization of the constructed functional $J(w,F)$.

Now, we explain how points of the minimum of the functional (25) are coupled with a solution of the problems (20), (24). For this purpose, we introduce a definition of a weak solution.

A pair of functions $\{w,F\} \in M$ is called the weak solution of the problems (20), (24) if the following equation is satisfied

$$(\Delta w,\Delta\mu) - (L(w,F),\mu) = (q,\mu) \quad \forall\mu \in H_0^2(\Omega)\,. \tag{28}$$

Theorem 2. *Points of the functional (25) minimum are weak solutions of the problems (20), (24).*

Proof. Let $\{w,F\} \in M$ be one of the points of the functional minimum (25). Let $\eta = w + t\,\delta w \quad \delta w \in H_0^2(\Omega)$ and we choose $\xi = F + \delta F$, $\delta F \in H_0^2(\Omega)$ in such a way that $\{\eta,\xi\} \in M$, i.e. in the way that $\beta(w,F,\mu) = 0$, $\forall\mu \in H_0^2(\Omega)$. Then, $J(w,F) \leq J(\eta,\xi)$, and hence we obtain

$$t\,(\Delta w,\Delta\delta w) + (\Delta F,\Delta\delta F) - t\,(q,\delta w) + \frac{t_2}{2}\,\|\,\Delta\delta w\,\|_{2,\Omega}^2 + \frac{1}{2}\,\|\,\Delta\delta F\,\|_{2,\Omega}^2 \geq 0,$$
$$\forall t \in R,\quad \delta w \in H_0^2(\Omega)\,, \tag{29}$$

and the condition $\beta(\eta,\xi,\mu) = 0$, taking $\mu = F$, yields

$$(\Delta F,\Delta\delta F) = -t\,(L(w,\delta w),F) - \frac{t^2}{2}\,(L(\delta w,\delta w),F)\,. \tag{30}$$

Substituting (30) in (29), dividing the obtained formula by t, and transiting into a limit for $t \to 0$, we get

$$(\Delta w,\Delta\delta w) - (L(w,F),\delta w) \geq (q,\mu)\,. \tag{31}$$

Substituting δw by $-\delta w$ in (31), we obtain (28).

Let us introduce the following notation

$$(\Phi(w,F),\mu) = a_1(\Delta w,\Delta\mu) - (L(w,F),\mu) - (q,\mu)\,.$$

Formula (28) can be presented in the following way

$$(\Phi(w,F),\mu) = 0, \tag{32}$$

and it is clear that $\Phi(w,F) \in H^{-2}(\Omega)$.

Therefore, each point of the minimum of the functional (28) on M satisfies (32), and hence it is the weak solution of the problems (19), (20). ■

Based on the proved theorems, one can say that the solution of the problems (19), (20) is equivalent to the solution of the problem of minimization (26) under constraints $\{w,F\} \in M$. In order to solve the problem in practice, one can employ numerous methods of searching for a minimum. Depending on the choice of the method of solution of the extremum problem, different algorithms can be constructed to find solutions of problems (19), (20).

Here we employ the method of gradient projection, which allows, under linear constraints, for essential simplification of the problem [56].

Let us construct an iterational process of minimization of $J(w,F)$ on M under the following scheme:

(a) element $w_0 \in H_0^2(\Omega)$ is chosen in an arbitrary way;

(b) after computation of w_n, we find $F_n \in H_0^2(\Omega)$ and $w_{n+1} \in H_0^2(\Omega)$ as solutions to the following problems

$$\beta(w_n,F_n,\mu) = 0,\quad F_n \in H_0^2(\Omega)\ \forall\mu \in H_0^2(\Omega)\,, \tag{33}$$
$$(\Delta w_{n+1},\Delta\mu) = (\Delta w_n,\Delta\mu) - \rho_n(\Phi(w_n,F_n),\mu) \quad \forall\mu \in H_0^2(\Omega)\,; \tag{34}$$

(c) the coefficient ρ_n in the step (b) is chosen from the following condition

$$J(w_{n+1},F_{n+1}) - J(w_n,F_n) \leq \varepsilon(\Phi(w_n,F_n),w_{n+1} - w_n),\quad 0 < \varepsilon < 1, \tag{35}$$

where ε plays the role of a parameter of the method.

Theorem 3. *For iterational process (33)–(34), $(\Phi(w_n,F_n),\mu) \to 0$ for $n \to 0$ and for an arbitrary point $\{w_0,F_0\} \in M$. The series $\{w_n,F_n\}$ obtained in this process includes a subseries convergent to the weak solution to the problems (19), (20).*

Proof. The possibility of constructing the series $\{w_n, F_n\}$ follows from the observation that $\forall \rho_n w_{n+1} \in H_0^2(\Omega)$ and, consequently, $L(w_{n+1}, w_{n+1}) \in H^{-2}(\Omega)$, $\nabla_k^2 w_{n+1} \in H^{-2}(\Omega)$ [57]. It means that the equation of coupling $\beta(w_{n+1}, F_{n+1}, \mu) = 0$ is solvable.

Consider the following difference

$$\Delta J_n = J(w_{n+1}, F_{n+1}) - J(w_n, F_n) = \frac{1}{2}(\Delta(w_{n+1} - w_n), \Delta(w_{n+1} + w_n)) + \frac{1}{2}(\Delta(F_{n+1} - F_n), \Delta(F_{n+1} + F_n)) - (q, w_{n+1} - w_n). \tag{36}$$

Since $\{w_n, F_n\} \in M$, $\{w_{n+1}, F_{n+1}\} \in M$ yields

$$\Delta J_n = (\Phi(w_n, F_n), \delta w) + \frac{1}{2}\|\Delta\delta w\|_{0,\Omega}^2 + \frac{1}{2}\|\Delta\delta F\|_{0,\Omega}^2,$$

where $\delta w = w_{n+1} - w_n$, $\delta F = F_{n+1} - F_n$. Formula (34) implies that δw stands for a general solution to the following boundary value problem $\Delta^2 \delta w = -\rho_n \Phi(w_n, F_n)$, $\delta w \in H_0^2(\Omega)$.

Hence

$$\delta w = -\rho_n G[\Phi(w_n, F_n)], \tag{37}$$

where $G[\bullet] : H^{-2}(\Omega) \to H_0^2(\Omega)$ is a linear bounded operator, which is inverse to the operator $\Delta^2(\bullet)$. Therefore,

$$\Delta J_n = -\rho_n (\Phi(w_n, F_n), G[\Phi(w_n, F_n)]) + \frac{1}{2}\|\Delta\delta w\|_{0,\Omega}^2 + \frac{1}{2}\|\Delta\delta F\|_{0,\Omega}^2. \tag{38}$$

Let us consider the second-order terms. We choose $\mu = \delta w$ in (34) and using (37) we get

$$\|\Delta\delta w\|_{0,\Omega}^2 = -\rho_n (\Phi(w_n, F_n), \delta w) = \rho_n^2 (\Phi(w_n, F_n), G[\Phi(w_n, F_n)]). \tag{39}$$

Let us estimate the last term of (38). Since $\{w_n, F_n\} \in M$ and $\{w_{n+1}, F_{n+1}\} \in M$, δF should satisfy the following equation

$$(\Delta\delta F, \Delta\mu) + (L(w_n, \delta w), \mu) + (\nabla_k^2 \delta w, \mu) + \frac{1}{2}(L(\delta w, \delta w), \mu) = 0, \quad \delta F \in H_0^2(\Omega), \quad \forall \mu \in H_0^2(\Omega).$$

Therefore, in particular, we get [31]

$$\|\Delta\delta F\|_{0,\Omega} \le c_7 \left(\left\| L(w_n, \delta w) \right\|_{L^1(\Omega)} + \|L(\delta w, \delta w)\|_{L^1(\Omega)} + \left\| \nabla_k^2 \delta w \right\|_{L^1(\Omega)} \right).$$

However, w_n belongs to a bounded set in $H_0^2(\Omega)$ for arbitrary n. Consequently, $\|\Delta\delta F\|_{0,\Omega} \le c_8 \|\Delta\delta w\|_{0,\Omega}^2$ or

$$\|\Delta\delta F\|_{0,\Omega}^2 \le c_9 \rho_n^4 (\Phi(w_n, F_n), G[\Phi(w_n, F_n)])^2. \tag{40}$$

Substituting (39), (40) into (38) and taking into account a positive definite (in the sense $(\Phi(w_n, F_n), G[\Phi(w_n, F_n)]) \ge \alpha \|\Phi(w_n, F_n)\|^2$) and boundedness of the operator $G[\bullet]$, one gets

$$\Delta J_n \le -\rho_n c_{10} \left\| \Phi(w_n, F_n) \right\|^2 \left(-1 + \frac{\rho_n}{2} + c_1 \frac{\rho_n^3}{2} \left\| \Phi(w_n, F_n) \right\|^2 \right).$$

The latter estimation shows that there exist values $\rho_n \neq 0$, which satisfy the inequality (35). For this purpose, one can choose ρ_n to satisfy the condition

$$\frac{\rho_n}{2} + c_1 \frac{\rho_n^3}{2} \left\| \Phi(w_n, F_n) \right\|^2 \le 1 - \varepsilon.$$

This can be done always since $0 < \varepsilon < 1$. Choosing ρ_n according to the given algorithm, the following inequality holds on each step

$$\Delta J_n \le -\rho_n \varepsilon \left\| \Phi(w_n, F_n) \right\|^2, \tag{41}$$

i.e. for arbitrary n, we have $J_{n+1} - J_n \le 0$. Since the functional J is bounded from below, the latter inequality implies that for $n \to \infty$ $\Delta J_n \to 0$. Besides, the inequality (41) yields the following estimation

$$\left\| \Phi(w_n, F_n) \right\|^2 \le \frac{-\Delta J_n}{\varepsilon \rho_n}. \tag{42}$$

It should be emphasized that the given algorithm for the choice of ρ_n guarantees that for arbitrary n we have $\rho_n \ge \rho_0 > 0$. Indeed, since $\Delta J_n \le 0$, we have

$$J(w_n, F_n) \le J(w_0, F_0) = A. \tag{43}$$

It follows from (43), that the norms $\|w_n\|_{2,\Omega}$, $\|F_n\|_{2,\Omega}$ are bounded. This implies boundedness of the norm $\left\| \Phi(w_n, F_n) \right\|$. The latter observation and (42) imply $\left\| \Phi(w_n, F_n) \right\| \to 0$ for $n \to \infty$, and consequently also $(\Phi(w_n, F_n), \mu) \to 0$ for $n \to \infty$ $\forall \mu \in H_0^2(\Omega)$.

The occurrence of a convergent subseries follows from the boundaries of the norms $\|w_n\|_{2,\Omega}$, $\|F_n\|_{2,\Omega}$ (see proof of Theorem 1). ■

Above, we have proved the convergence of the procedure of reduction of the input system (19) to a successive solution of the bi-harmonic equation of the Germain–Lagrange type.

In what follows, we employ a method of variational iterations to solve the bi-harmonic Germain–Lagrange equation. Observe that the method of variational iterations has been employed on each step of the iterational procedure [58]. The method of variational iterations (MVI) is a modified variant of the Kantorovich method [59,60] and it allows for the improvement of the system of coordinate functions when the computational process is carried out in all directions.

This method allows for changing the form of the load and boundary conditions. Problems regarding convergence of MVI have been considered by Kirichenko [61] and, more recently, in Ref. [40]. For instance, the method has been employed in Refs. [60,62] to study contact interactions of plates and bending of plates, taking the account of different materials moduli and physical non-linearity.

Now, let us illustrate advantages of the MVI based on solutions to the case studies [63], which are obtained from the systems (17), (18).

We illustrate the process of finding the solutions by using the following equation

$$Aw(x, y) = q(x, y); x, y \in \Omega(x, y), \tag{44}$$

where A is a certain operator defined on the set $D(A)$ of the Hilbert space $L_2(\Omega)$; $q(x, y)$ is a given function, $w(x, y)$ stands for the function being searched; $\Omega(x, y)$ is the space of possible changes of the variables x and y.

If $\Omega(x, y) = X \times Y$ (X — certain bounded set of the variable x, Y — bounded set of the variable y), then the solution to Eq. (44) takes the form

$$w_N(x, y) = \sum_{i=1}^{N} u_i(x) v_i(y), \tag{45}$$

where the functions $u_i(x)$ and $v_i(y)$ are found from the below system of the equations (they do not have to satisfy the boundary conditions)

$$\begin{aligned} &\int_X (Aw_N - q) u_1(x)\, dx = 0, \qquad \int_Y (Aw_N - q) v_1(y)\, dy = 0, \\ &\cdots\cdots\cdots\cdots\cdots\cdots\cdots\cdots\cdots\cdots\cdots\cdots\cdots\cdots\cdots\cdots \\ &\int_X (Aw_N - q) u_N(x)\, dx = 0, \qquad \int_Y (Aw_N - q) v_N(y)\, dy = 0, \end{aligned} \tag{46}$$

in the following way: if there is a system of N functions given with respect to one variable, for instance, $u_1^0(x), u_2^0(x), \ldots, u_N^0(x)$; then the first N equations of the system (46) define a system of N functions $v_1^1(x), v_2^1(x), \ldots, v_N^1(x)$; the obtained functions stand for the new choice of the functions with respect to the variable x – $u_1^2(x), u_2^2(x), \ldots, u_N^2(x)$; the given choice defines new functions with respect to the variable y – $v_1^3(x), v_2^3(x), \ldots, v_N^3(x)$, and so on. Therefore, although the functions can be given in an arbitrary way in the beginning, they are successively improved in the computational MVI process. This allows one to choose the initial approximation in an arbitrary way. We consider the MVI

Table 1
Deflections of the centre $w(0.5;0.5)$ of one-layer plate for $q(x,y)=50$.

Method	Boundary conditions	
	(47)	(48)
MVI [40]	0.2030	0.06483
Exact solution [63]	0.2028	0.0631

procedure based on an example. We use the introduced theory to find solution of the bi-harmonic equation $A_i w_i(x,y) = q(x,y)$, where the operator $A_i w_i(x,y)$ takes the following form

$$A_i w_i(x,y) = D\left[\frac{\partial^2}{\partial x^2}\left(\frac{\partial^2 w_i}{\partial x^2}+\frac{\partial^2 w_i}{\partial y^2}\right)+\frac{\partial^2}{\partial y^2}\left(\frac{\partial^2 w_i}{\partial x^2}+\frac{\partial^2 w_i}{\partial y^2}\right)\right],$$

where $D=\frac{E_i h^3}{12\left(1-\nu_i^2\right)}$ is the cylindrical stiffness, E_i is Young's modulus, and ν_i stands for the Poisson's ratio.

We consider two boundary conditions:

(a) simple support:

$$w_i\big|_{\partial\Omega_i}=\frac{\partial^2 w_i}{\partial n^2}\Big|_{\partial\Omega_i}=0,\quad i=1,2, \tag{47}$$

(b) clamping:

$$w_i\big|_{\partial\Omega_i}=\frac{\partial w_i}{\partial n}\Big|_{\partial\Omega_i}=0,\quad i=1,2, \tag{48}$$

for the domain $\Omega=(0,a)\times(0,b)$, where $\partial\Omega$ is the border of Ω.

PDE and the mentioned boundary conditions are recast to the counterpart non-dimensional form by means of the relations:

$$x=\bar{x}a,\ y=\bar{y}b,\ w=\bar{w}h,\ \lambda=a/b=1,$$
$$\bar{q}(x,y)=\frac{q(x,y)}{12(1-\nu^2)}\frac{a^4}{Eh^4},\ \nu=0.3.$$

As the initial approximations for two employed types of the boundary conditions, we use the functions $w_1(x)$, $w_2(y)$, which do not satisfy the boundary conditions, i.e. $w_1(x)=1$; $w_2(y)=1$. The iterational MVI procedure was terminated already on the 4th step of the variational iterations. The obtained results are presented in Table 1.

It should be noted that we obtained full coincidence with the exact solution (in the case of the boundary condition (4)/(5) the obtained difference is 0.1%/0.6%).

It should be emphasized that the iterational procedure (22) linearizes and decreases the order of the input system of equations. Furthermore, it can be extended to solve the problem (17), (18).

In order to validate the employed procedure aimed at reducing the problem to that of finding a solution to the bi-harmonic equation, the comparative computations were carried out by employing the finite element method (FDM), the finite element method of (FEM), and the variational iterations method (MVI).

Observe that the employment of MVI results in the simplification of the obtained system of bi-harmonic equations by reducing the problems to solving ODEs on each step of the iterational MVI procedure. Let us employ this method to solve our problem. For this purpose, the searched functions of two variables are taken in the following scalar product form

$$w(x,y)=w_1(x)\cdot w_2(y),\ F(x,y)=F_1(x)\cdot F_2(y). \tag{49}$$

Knowing $w_2(x)$, $F_2(x)$, we define $w_1(x)$, $F_1(x)$. For this purpose, we substitute (49) into (22), and we employ the Bubnov–Galerkin procedure along the direction y. The following ODEs are obtained:

$$\begin{aligned} &A_1 w_1^{IV}(x)+B_1 w_1^{II}(x)+C_1(x)w_1(x)=D_1(x),\\ &\tilde{A}_1 F_1^{IV}(x)+\tilde{B}_1 F_1^{II}(x)+\tilde{C}_1(x)F_1(x)=D_1(x).\end{aligned} \tag{50}$$

The associated boundary conditions follow

$$w_1(x)=0,\ w_1^{II}(x)=0,\quad x=0,\ 1, F_1(x)=0,\quad F_1^{II}(x)=0,\quad x=0,\ 1. \tag{51}$$

Solving (50) with the boundary conditions (46) by an arbitrary numerical method, we find $w_1(x)$, $F_1(x)$. We consider the obtained values of $w_1(x)$, $F_1(x)$ as the approximating functions, and then carry out the Bubnov–Galerkin procedure [64] along the direction x. The following ODEs are obtained to find $w_2(x)$, $F_2(x)$:

$$\begin{aligned} &A_2 w_2^{IV}(y)+B_2 w_2^{II}(y)+C_2(y)w_2(y)=D_2(y),\\ &\tilde{A}_2 F_2^{IV}(y)+\tilde{B}_2 F_2^{II}(y)+\tilde{C}_2(y)F_2(y)=D_2(y),\end{aligned} \tag{52}$$

and the supplemented boundary conditions follow

$$w_2(y)=0,\ w_2^{II}(y)=0,\quad y=0,\ 1, F_2(y)=0,\quad F_2^{II}(y)=0,\quad y=0,\ 1. \tag{53}$$

Solving (52) with the boundary conditions (53), we find $w_2(x)$, $F_2(x)$. In this way, one step of the variational iterations is completed. In the next steps, the procedure of finding $w_1(x)$, $F_1(x)$, and then $w_2(x)$, $F_2(x)$ is repeated.

After completing all steps of the variational iterations, the obtained results accuracy is estimated. The final expression for the shell deflection is:

$$w(x,y)=w_1^{(k-1)}(x)\cdot w_2^{(k)}(y),\ F(x,y)=F_1^{(k-1)}(x)\cdot F_2^{(k)}(y), \tag{54}$$

where k stands for the number of the variational iteration.

The coefficients A_i, B_i, C_2, D_2 for both equations for $w_i(x)$ take the following form:

$$\begin{aligned} &A_1=\int_0^1 w_2^2(y)dy,\quad B_1=\int_0^1 w_2^{II}(y)w_2(y)dy,\quad C_1=\int_0^1 w_2^{IV}(y)w_2(y)dy,\\ &D_1(x)=\int_0^1\{q(x,y)+L(w(x,y),F(x,y))\}w_2(y)dy,\qquad \underset{(1,2)}{\longleftrightarrow}\end{aligned} \tag{55}$$

In fact, the simultaneous employment of the iterational procedure and the MVI for the system (22) enables one to:

(1) reduce the order of the system by half, i.e. from the 8th to the 4th order;
(2) carry out linearization of the non-linear systems being searched;
(3) transit PDEs to ODEs with constant coefficients.

This can be viewed as a serious achievement in the field of non-linear PDE of elliptic type. The given approach is illustrated by an example devoted to the computation of flexible isotropic plates with constant thickness and a square planform, taking into account the following three boundary conditions

$$w|_\Gamma=\frac{\partial^2 w}{\partial n^2}\Big|_\Gamma=F|_\Gamma=\frac{\partial^2 F}{\partial n^2}\Big|_\Gamma=0, \tag{56}$$

$$w|_\Gamma=\frac{\partial^2 w}{\partial n^2}\Big|_\Gamma=F|_\Gamma=\frac{\partial F}{\partial n}\Big|_\Gamma=0, \tag{57}$$

$$w|_\Gamma=\frac{\partial w}{\partial n}\Big|_\Gamma=F|_\Gamma=\frac{\partial F}{\partial n}\Big|_\Gamma=0. \tag{58}$$

In order to simplify the computations, we employ MVI only in the first approximation ($N=1$). The system of ODEs is reduced to AEs (algebraic equations) by the finite difference method (FDM) with approximation $0(h^2)$, which is then solved by the Gauss method. The integration interval [0, 1] is divided into 100 parts.

The dependence $q[w(0.5,0.5)]$ is shown in Fig. 2. Curves 1, 2, and 3 correspond to boundary conditions (56), (57), and (58), respectively. The curves 2 and 3 are obtained for Poisson's ratio $\nu=0.33$, whereas the curve 1 — for $\nu=0.1$. In the figure, circles refer to the experimental results [65] while stars are associated with the solution obtained by the FDM [64], which is applied directly to equations (2.16) (mesh 20×20), and the obtained system of non-linear algebraic equations is solved with the help of Newton's method (the curve 4 corresponds to the solution obtained by FEM with the help of the procedure (22)). The studied area of the plate is approximated with 30 triangular elements.

Fig. 2. The function $q\,[w(0.5, 0.5)]$.

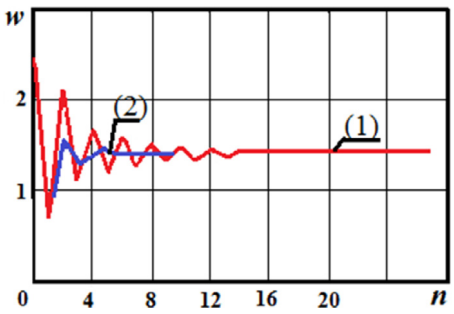

Fig. 3. Deflection of the plate centre vs. the number of iterations performed: 1 — regular number of iterations; 2 — reduced number of iterations.

The computation was carried out with the step $\Delta q = 10$, and in order to accelerate the iterational procedure, the values of w and F, obtained in the previous step under a continuous increase in the load, served as the initial approximations.

The spatial step (in FEM and FDM) was chosen in a way to obtain satisfying convergence of the obtained results. The presented results are obtained for a rectangular plate by using the MVI. The dependence of the deflection of the plate centre on the number of iterations n is reported in Fig. 3 (curve 1) for the boundary condition (45). The remaining parameters have the following values: the number of the mesh partitions $N = 20$; $q = 60$, $\nu = 0.28$, the assumed computational accuracy $\varepsilon = 10^{-3}$. In order to obtain a solution with the required accuracy, 26 iterations were performed.

One can conclude from Fig. 3 that the plate deflection oscillates around and then continuously approaches a certain average value. The explanation of such an observation is as follows. Since the initial approximation is yielded by a solution to the linear problem, the plate deflection is higher than its counterpart real value. Substituting $w(x, y)$ in the second equation of the system (27) yields a higher value of the stress function than the real value. This is why the stress function $F(x, y)$ generates a lower value of the deflection obtained from the first equation of the system (27). It means that the deflection on the odd (even), iteration is larger (smaller). This observation allows one to obtain convergence of the iterational process sooner if the deflection after iteration is defined by the following formula

$$w = \frac{w_{even} + w_{odd}}{2}. \tag{59}$$

Owing to application of the formula (59), we reduced the number of iterations to eight (curve 2 in Fig. 3) for all employed boundary conditions. An increase in the load implies a decrease in the convergence of the numerical results (in particular, in the case of free support).

Now, we employ the so far presented scheme to study equation (17), the solutions of which are assumed to be

$$W_j = \sum_{k=1}^{m} X_{1k}(x)Y_{1k}(y), \qquad \Phi_j = \sum_{k=1}^{m} X_{2k}(x)Y_{2k}(y).$$

Physical non-linearity is taken into account with the help of the method of variable parameters of stiffness, proposed by Birger [65]. Convergence of the latter approach was proved by Umanskiy [66].

In this case, Young's modulus $E = E(x, y, z, e_i)$ and Poisson's ratio $\nu = \nu(x, y, z, e_i)$ depend on the stress–strain body state in its each point, and the following relations hold

$$E = \frac{9kG}{3k + G}, \qquad \nu = \frac{1}{2}\frac{3k - 2G}{2k + G}, \tag{60}$$

where k stands for the coefficient of the volume deformation and it has a constant value.

The shear modulus G is defined by the relation

$$G = \frac{1}{3}\frac{\sigma_i(\varepsilon_i)}{\varepsilon_i},$$

where ε_i is the deformations intensity, and σ_i is the stress intensity. In this case, the following formula holds

$$\varepsilon_i = \frac{3}{2}\left[\left(\varepsilon^z_{xx} - \varepsilon^z_{yy}\right)^2 + \left(\varepsilon^z_{yy} - \varepsilon^z_{zz}\right)^2 + \left(\varepsilon^z_{xx} - \varepsilon^z_{zz}\right)^2 + \frac{3}{2}\varepsilon^z_{xy}\right]^{\frac{1}{2}}.$$

The deformation diagram $\sigma_i = \sigma_i(e_i)$ is bi-linear and satisfies the following equations:

$$\sigma_i = 3G_0\varepsilon_i, \qquad \varepsilon_i < \varepsilon_s, \qquad \sigma_i = 3G_0\varepsilon_s + 3G_i(\varepsilon_i - \varepsilon_s), \qquad \varepsilon_i \geq \varepsilon_s.$$

The method of variable parameters belongs to the methods of successive approximations. The shell is divided into $N \times N$ parts of the plane and m layers with respect to the shell thickness. A 3D mesh is obtained and each of the nodes should be coupled with the parameters E and ν to be defined. In the initial approximation, the parameters of elasticity E and ν are chosen as $E = E_0$ and $\nu = \nu_0$. Then, the problem (2.6)–(2.7) is solved with the help of MVI. As a result, w and Φ are found. Next, ε_i and σ_i are calculated. After that, the parameters E and ν are obtained again from (60). The procedure of computation of E and ν is repeated unless the condition $\frac{E_{k+1} - E_k}{E_k} \leq \varepsilon_p$ is satisfied, where ε_p stands for the given accuracy of the final estimation of E, and E_k means the value of E in its kth approximation. In further computations, the module of volume deformation is taken as 1.94, and $E_0 = 2.56$, $\nu_0 = 0.28$.

In the numerical experiment, we investigate the mathematical model of corrosion wear of the plate, i.e. we take $k_x = 0$ and $k_y = 0$ in Eqs. (17) and (18). The mathematical model of corrosion wear of the studied plate can be understood as a set of relations governing its stress–strain state versus external input. However, the interaction of the metals with aggressive environment requires a series of important characteristics to be taken into account and the stress damage caused by corrosion wear is called "corrosion under stress". On the other hand, the stress–strain state depends on the magnitude of the initial stress and boundary conditions as well as on the cyclic character of the applied load. One can observe the localization of the corrosion process in the plate parts with largest stresses, damage of the surface layers as well occurrence and damage of the material homogeneity.

In this paper, we employ mathematical models, in which the depth of corrosion damage δ depends on time and on the stress–strain of the plate material, i.e. we take $\delta = f\left(t, \sigma_{ij}, \sigma_i\left(\varepsilon_i\right)\right)$, where δ is the depth of the material corrosion damage, σ stands for the stress amplitude in the plate element, and t denotes time.

An increase in the corrosion depth δ results in an increase in σ due to a decrease in the object's thickness h, which accelerates the corrosion wear process. We employ two models to study dynamics of a plate embedded in an aggressive environment.

I model (Dolinskii model [17]):

$$\frac{\partial\delta}{\partial t} = \varphi(t)(1 + k\sigma_i), \tag{61}$$

where: $\varphi(t) = (a + b\exp(\beta t - 1)) / \exp(\beta t)$; σ_i — stress intensity; a, b — coefficients obtained experimentally.

II model (Gutman model [19]):

$$\frac{\partial\delta}{\partial t} = V(t)\exp\left(\gamma\sigma_0\right), \tag{62}$$

where: σ_0 — averaged stress; $V(t) = \alpha \exp(\mu t)$ — non-dimensional function of time; γ, α, μ — experimentally estimated coefficients.

Let us consider duralumin EN AW-2024 with the following parameters:

$a = 0.44$ mm/year, $b = 0.153$ mm/year, $\beta = 0.2$ year $^{-1}$,

$k = 0.0089$ (MPa)$^{-1}$, $\alpha = 0.48$ mm/year, $\eta = 0.091$ year $^{-1}$,

$\gamma = 0.00588$ (MPa)$^{-1}$, $V_0 = 0.217$ mm/year, $\gamma = 0.00047$ (MPa)$^{-1}$, $E = 7.5 \cdot 10^5$ kg cm^2.

We aim to find how these two models can be used to predict dynamic behaviour of the plate under the action of an aggressive environment.

A mesh is applied to the whole volume of the plate and the following two boundary conditions are employed to carry out numerical study:

1. Simple support

$$w = M_{xx} = N_{xx} = N_{xy} = 0, \qquad x = 0, a,$$

$$w = M_{yy} = N_{yy} = N_{xy} = 0, \qquad y = 0, b;$$

2. Movable clamping

$$w = \frac{\partial w}{\partial x} = N_{xx} = N_{xy} = 0, \qquad x = 0, a,$$

$$w = \frac{\partial w}{\partial y} = N_{yy} = N_{xy} = 0, \qquad y = 0, b.$$

The plate is loaded by the uniformly distributed load q until the load reaches a half of σ_s (plastic flow limit). Then, from one side, the plate subjected to the fixed load is embedded in an aggressive environment. The oxidation takes place until σ_i (stress intensity) achieves the strength of material limit σ_{pr}. The plate stress–strain state is defined on each time step t, and then the values of w and F are estimated with the help of MVI.

The corrosion wear is quantified based on the model I and II. Both these models allow for construction of a dependence between the corrosion wear depth $\delta(x, y, t)$ and the plate stress–strain state. In the aggressive environment, the plate thickness h changes in time and the magnitude of its decrease $\mu(x, y, t)$ is estimated in all mesh points with the help of the stress–strain characteristics. The following parameters are fixed: initial volume $V = 0.749$, Young's modulus $E = 2.56$, Poisson's ratio $\nu = 0.28$, and $G_1 = 0.57$, $k_x = k_y = 0$ in (17) and (18).

Remark. Convergence of the MVI in Eqs. (19) has been proved in Ref. [67] (without the linearization method and dimension reduction).

5. Numerical experiments

Case study 1. For fixed $\lambda_1 = \frac{a}{h} = 20$, plates with two boundary conditions, i.e. simple support and movable clamping, are considered. Plates are uniformly loaded by transverse load up to the value of q, which corresponds to $^1/_2$ of the plastic flow limit (for $\lambda_1 = 20$ this value is equal to $q = 1.4$). Furthermore, for fixed q, the plates are put into an oxidable environment. Owing to the model I (II), the simply supported plate decreases its volume by 51% (48%) after 168 (62) months (curve 2 (4) in Fig. 4). The threshold point responsible for the damage is reached when σ_i reaches the material strength σ_{pr}. One can notice that both models of plates reach the threshold with very close value of V (the difference is 3%). In the case of movable clamping, the plate of the model I (II) reaches the material strength limit after 174 (82) months, which corresponds to curve 1 (4) in Fig. 4.

Boundary conditions affect the rate of the plate damage. If we compare how the models work, it is interesting to note that both plates reach the strength material limit with very close values of the volume V (with a difference of 3%). However, the corrosion damage estimated based on the model I takes place at (about 2.5 times) slower rate than in the case of the model II.

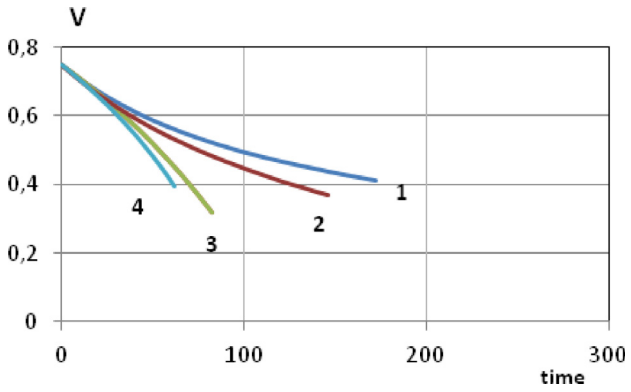

Fig. 4. Plate volume vs. time for $\lambda_1 = 20$: curve 1 — movable clamping of the model I; 2 — simple support of the model I; 3 — movable clamping of the model II; 4 — simple support of the model II.

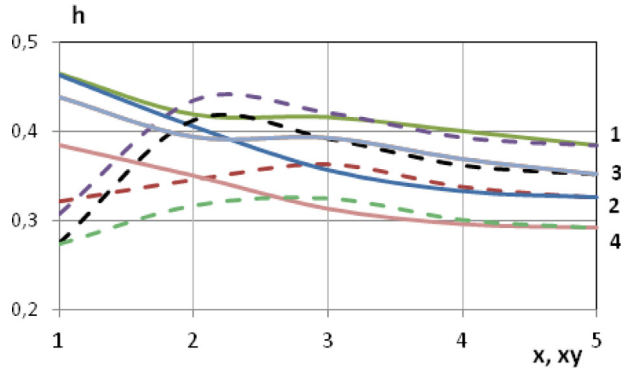

Fig. 5. Change in the thickness h, based on the model I; solid curves concern changes in h along the axial axis $y = 0.5$, $0 \le x \le 0.5$ whereas dashed curves present changes in h along the diagonal xy: curve 1 — movable clamping $\lambda_1 = 20$; 2 — simple support $\lambda_1 = 20$; 3 — movable clamping $\lambda_1 = 40$; 4 — simple support $\lambda_1 = 40$.

The change in the thickness h ($y = 0.5$, $0 \le x \le 0.5$) along the line $0X$ (solid curves) and along the diagonal (dashed curves) are shown in Fig. 5.

Curves 1 (Fig. 5) illustrate the change in the thickness h at the time instant when the plate reaches the material strength limit along the diagonal (dashed curves) and along line $0X$ (solid curves) based on the model I with movable clamping. Curves 2 (Fig. 5) exhibit the change in the h along the axial line $0X$ for movable clamping due to the model I. In this case, the thickness of the plate decreases more in the corner than in the centre of the plate. In the case of simple support, a significant decrease in the thickness h takes place on both the plate edge and in the centre.

However, an opposite observation can be made in the case of the model II. Namely, for movable clamping, the corrosion process takes place more intensively and the plate thickness h in the centre decreases twice (curve 1 in Fig. 6). In the case of simple support (curve 2 in Fig. 6), the values of h coincide with the change in the thickness for the same conditions but for model I.

The stress state σ_i of the bottom layer of the plate reaches $\sigma_i(0.5; 0.5) = 1.15$ in the centre of the plate for the simple support and the model I (Fig. 7), and $\sigma_i(0.5; 0.5) = 1.105$ for the model II (Fig. 8). At the time instant when the material strength limit is achieved, the character of the stress process essentially differs with respect to the axial line $0X$ and the diagonal XY. In particular, different values of σ_i are exhibited along the diagonal (dashed curves 2 in Figs. 7 and 8).

Case study 2. The problem is solved for $\lambda_1 = \frac{a}{h} = 40$. Two kinds of boundary conditions are considered: simple support and movable

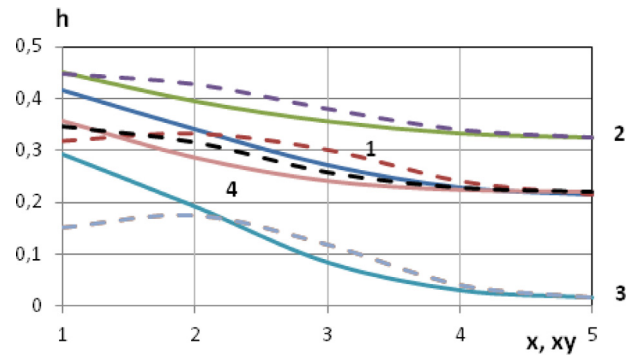

Fig. 6. Change in the thickness h, based on the model II; solid curves concern the change in h along the axial axis $y = 0.5$, $0 \le x \le 0.5$ whereas dashed curves present changes in h along the diagonal xy: curve 1 — movable clamping $\lambda_1 = 20$; 2 — simple support $\lambda_1 = 20$; 3 — movable clamping $\lambda_1 = 40$; 4 — simple support $\lambda_1 = 40$.

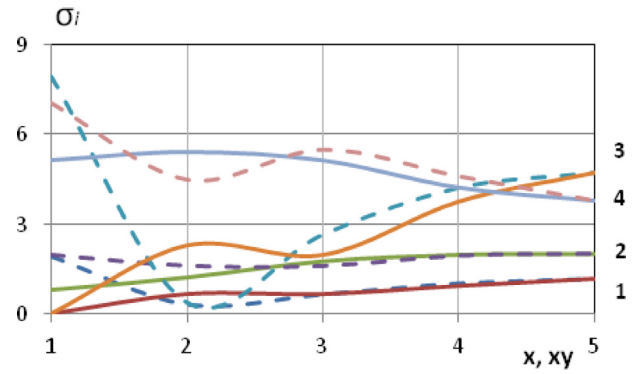

Fig. 7. Stress state σ_i of the bottom layer of the plate, based on the model I: solid curves represent changes in σ_i along the axial axis $y = 0.5$, $0 \le x \le 0.5$ whereas dashed curves present changes in σ_i along the diagonal xy: curve 1 — movable clamping $\lambda_1 = 20$; 2 — simple support $\lambda_1 = 20$; 3 — movable clamping $\lambda_1 = 40$; 4 — simple support $\lambda_1 = 40$.

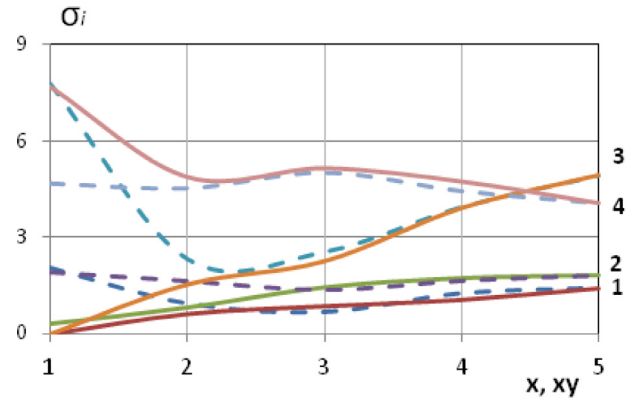

Fig. 8. Stress state σ_i of the bottom layer of the plate, based on the model II: solid curves show changes in σ_i along the axial axis $y = 0.5$, $0 \le x \le 0.5$ whereas dashed curves present changes in σ_i along the diagonal xy: curve 1 — movable clamping $\lambda_1 = 20$; 2 — simple support $\lambda_1 = 20$; 3 — movable clamping $\lambda_1 = 40$; 4 — simple support $\lambda_1 = 40$.

clamping. Plates are loaded by the uniformly distributed load up to $q = 5$.

In the case of movable clamping, the plate reaches the material strength limit after 225 months with $V = 0.326$ for the model I (curve 1 in Fig. 9). In the case of model II, it happens after 78 months with $V = 0.285$ (curve 3 in Fig. 9). For simple support of the model I, the material strength limit is reached after 214 months with $V = 0.384$

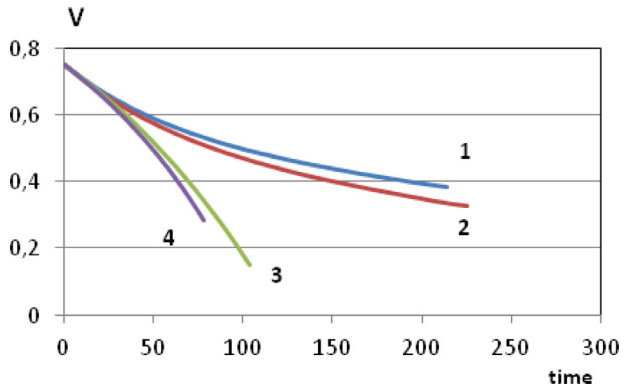

Fig. 9. Plate volume vs. time for $\lambda_1 = 40$: curve 1 — movable clamping of model I; 2 — simple support of model I; 3 — movable clamping of the model II; 4 — simple support of model the II.

(curve 2 in Fig. 9) and after 104 months with $V = 0.151$ for model II (curve 4 in Fig. 9).

Therefore, for plates with $\lambda_1 = 40$, the process of oxidation takes place twice faster for the model II and the difference between the threshold volumes for the model II is over twice smaller than in the case of model I.

The change in the plate thickness h depends on the chosen model. In the case of movable clamping, the thickness h in the plate centre decreases up to $h(0.5, 0.5) = 0.416$ (curves 3 in Fig. 5) for the model I, and up to $h(0.5, 0.5) = 0.016$ (curve 3 in Fig. 6) for the model II, before achieving the material strength limit. For simple support of the model I, $h(0.5, 0.5) = 0.296$ (curve 4 in Fig. 5) and $h(0.5, 0.5) = 0.4$ — model II (curves 4 in Fig. 6).

Based on the reported results, one can conclude that the decrease in the critical load, with simultaneous increase in λ_1, is of 50% and 10% for the model I and II, respectively. Besides, a general tendency is observed that an increase in the load q decreases the oxidation time, i.e. the material strength limit is reached faster.

The change in the intensity of stress σ_i (curves 1, 2) essentially depends on the chosen model (I or II) and the changes are exhibited along the diagonal XY and along the axis $0X$ (Figs. 7, 8).

Case study 3. (plates with $\lambda_1 = \frac{a}{h} = 50$). Two kinds of boundary conditions are considered: simple support and movable clamping. Plates are uniformly loaded by continuously distributed load up to $q = 6.1$.

In the case of movable clamping, the plate reaches the material strength limit after 135 months with $V = 0.434$ (model I, curve 1 in Fig. 10) and after 92 months with $V = 0.248$ (model II, curve 3 in Fig. 10). If simple support is considered, then the material strength limit is reached after 126 months with $V = 0.399$ (model I, curve 2 in Fig. 10) and after 66 months with $V = 0.359$ (model II, curve 4 in Fig. 10).

Therefore, in the case of plates with $\lambda_1 = 50$, the oxidation process is carried out 40% faster for the model II.

The change in the plate thickness h differs depending on the chosen model. In the case of movable clamping, after reaching the material strength limit, the thickness h of the centre of the plate decreases to $h(0.5, 0.5) = 0.39$ (curves 1 in Fig. 11) and to $h(0.5, 0.5) = 0.11$ (curves 1 in Fig. 12) for models I and II, respectively. In the case of simple support, it reaches $h(0.5, 0.5) = 0.351$ (curves 2 in Fig. 11) and $h(0.5, 0.5) = 0.3$ (curves 2 in Fig. 12), respectively.

A change in the stress σ_i intensity based on the numerical computations differs essentially between the model I (curves 1, 2 in Fig. 13) and model II (curves 1, 2 in Fig. 14) in both diagonal XY and axial $0X$ directions.

Case study 4. (plates $\lambda_1 = \frac{a}{h} = 100$). We consider two kinds of the boundary conditions: simple support and movable clamping. The studied plates are uniformly loaded by continuous load up to $q = 41$.

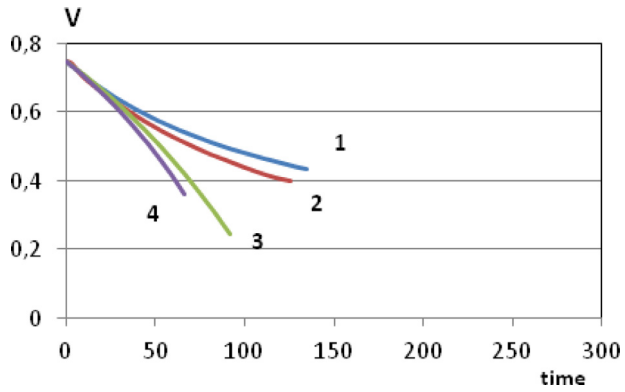

Fig. 10. Plate volume vs. time for $\lambda_1 = 50$: curve 1 — movable clamping of model I; 2 — simple support of the model I; 3 — movable clamping of the model II; 4 — simple support of the model II.

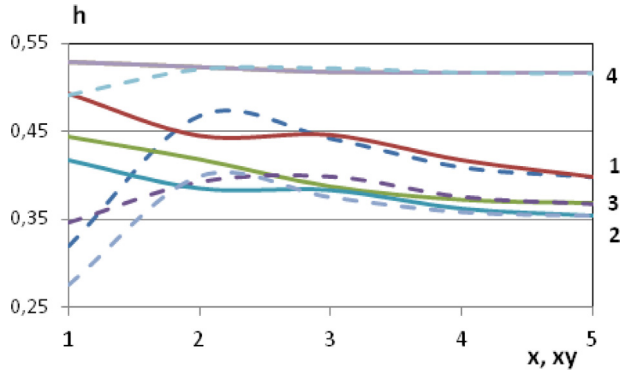

Fig. 11. Change in the thickness h based on the model I; solid curves depict changes in h along the axial axis $y = 0.5$, $0 \le x \le 0.5$ whereas dashed curves presents changes in h along the diagonal xy: curve 1 — movable clamping $\lambda_1 = 50$; 2 — simple support $\lambda_1 = 50$; 3 — movable clamping $\lambda_1 = 100$; 4 — simple support $\lambda_1 = 100$.

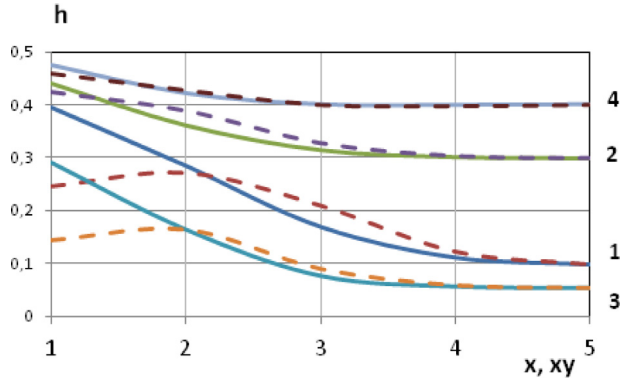

Fig. 12. Change in the thickness h based on the model II; solid curves depict changes in h along the axial axis $y = 0.5$, $0 \le x \le 0.5$ whereas dashed curves presents changes in h along the diagonal xy: curve 1 — movable clamping $\lambda_1 = 50$; 2 — simple support $\lambda_1 = 50$; 3 — movable clamping $\lambda_1 = 100$; 4 — simple support $\lambda_1 = 100$.

For the model I and the movable clamping, the plate reaches the limit of material strength (curve 1 in Fig. 15) after 271 months with $V = 0.375$, which stands for its initial volume. In the case of the plate model II, the material strength limit is reached after 108 months and $V = 0.117$ (curve 3 in Fig. 15). In the case of simple support and the model I, the material strength limit is reached after 74 months with $V = 0.521$ (curve 2 in Fig. 15) and after 60 months with $V = 0.421$ in the case of the plate model II (curve 4 in Fig. 15).

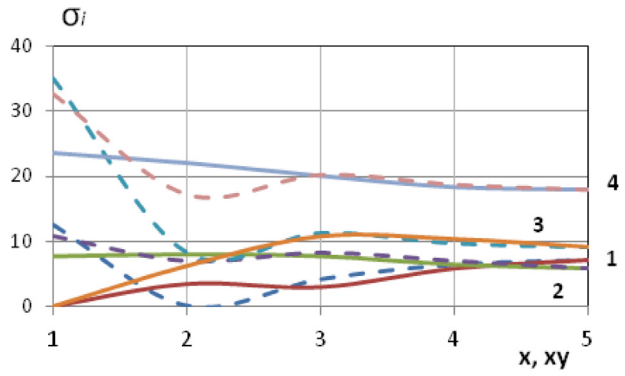

Fig. 13. Stress state σ_i of the bottom of the plate, based on the model I: solid curves show changes in σ_i along the axial axis $y = 0.5$, $0 \le x \le 0.5$ whereas dashed curves presents changes in σ_i along the diagonal xy: curve 1 — movable clamping $\lambda_1 = 50$; 2 — simple support $\lambda_1 = 50$; 3 — movable clamping $\lambda_1 = 100$; 4 — simple support $\lambda_1 = 100$.

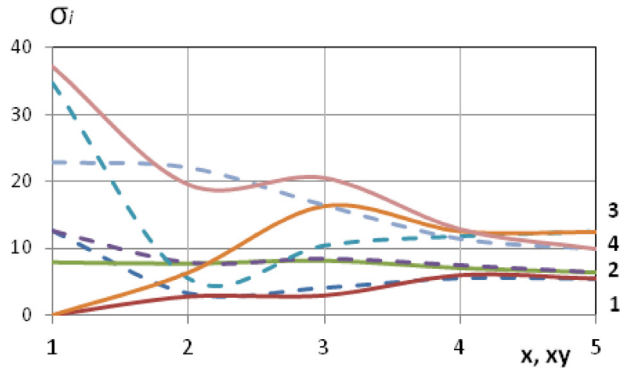

Fig. 14. Stress state σ_i of the bottom layer of the plate, based on the model II: solid curves show changes in σ_i along the axial axis $y = 0.5$, $0 \le x \le 0.5$ whereas dashed curves presents changes in σ_i along the diagonal xy: curve 1 — movable clamping $\lambda_1 = 50$; 2 — simple support $\lambda_1 = 50$; 3 — movable clamping $\lambda_1 = 100$; 4 — simple support $\lambda_1 = 100$.

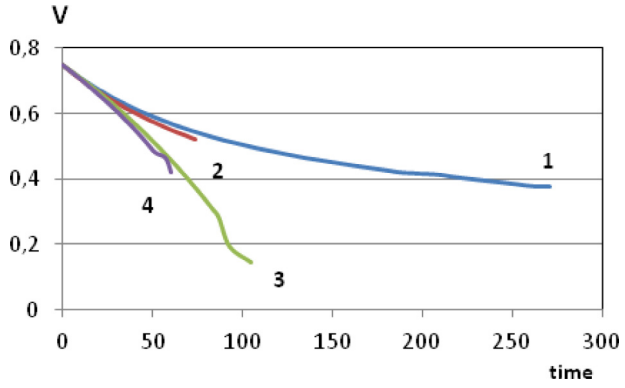

Fig. 15. Plate volume vs. time for $\lambda_1 = 100$: curve 1 — movable clamping of model I; 2 — simple support of model I; 3 — movable clamping of the model II; 4 — simple support of the model II.

Let us briefly summarize the obtained results. The change in the thickness of plates essentially depends on the chosen model. After achieving the material strength limit, the thickness h, measured in the centre of the plate, decreases to $h(0.5, 0.5) = 0.369$ (curves 3 in Fig. 11, model I) and to $h(0.5, 0.5) = 0.06$ (curves 3 in Fig. 12, model II). In the case of simple support, $h(0.5, 0.5) = 0.52$ (curves 4 in Fig. 11, model I) and $h(0.5, 0.5) = 0.4$ (curves 4 in Fig. 12, model II).

The change in the intensity of stresses σ_i is essentially different for the model I (curves 3, 4 in Fig. 13) and model II (curves 3, 4 in Fig. 14) and along the diagonal XY and the axis $0X$.

6. Concluding remarks

In this work, two mathematical models of flexible shallow shells have been derived, taking the account of the geometric non-linearity: (i) mathematical model under coupled temperature and deformation (equations in terms of displacements) fields; (ii) mathematical model taking into account also physical non-linearity. In both models, the one-sided corrosion wear has been taken considered in terms of Dolinskii and Gutman models.

We have proposed and successfully employed the method to decrease the order of the governing equations and to conduct their linearization by reduction of the problem to study the bi-harmonic equation.

In order to solve the reduced problem numerically, the method of variational iterations (MVI) and the method of variable stiffness parameter have been used.

It has been shown that the velocity of the decrease in the plate thickness depends essentially on the load. The change in plate thickness depends on the chosen (Dolinskii or Gutman) model. The studied plates reach the strength material limit practically with the same volume, but after different time intervals.

Declaration of competing interest

The authors declare that they have no known competing financial interests or personal relationships that could have appeared to influence the work reported in this paper.

Acknowledgement

This work has been supported by the Grant Russian Science Foundation (RSF), Russia No 16-11-10138-∏.

References

[1] M. Amabili, Non-linear vibrations of doubly curved shallow shells, Internat. J. Non-Linear Mech. 40 (5) (2005) 683–710.
[2] M. Amabili, Non-linearities in rotation and thickness deformation in a new third-order thickness deformation theory for static and dynamic analysis of isotropic and laminated doubly curved shells, Int. J. Non-linear Mech. 69 (2015) 109–128.
[3] M. Amabili, Nonlinear damping in nonlinear vibrations of rectangular plates: derivation from viscoelasticity and experimental validation, J. Mech. Phys. Solids 118 (2018) 275–292.
[4] E.Yu. Krylova, I.V. Papkova, A.O. Sinichkina, T.B. Yakovleva, V.A. Krysko-jr, Mathematical model of flexible dimension-dependent mesh plates, J. Phys. Conf. Ser. 1210 (2019) 012073.
[5] V.I. Eremeev, L.M. Zubov, Mechanics of Elastic Shells, Nauka, Moscow, 2008.
[6] E.Yu. Krylova, I.V. Papkova, V.A. Krysko, Theory of vibrations of carbon nanotubes like flexible micropolar mesh cylindrical shells taking into account shift, Izv. Saratov Univ. Ser. Math. Mech. Inf. 19 (3) (2019) 305–316.
[7] E. Carrera, S. Brischetto, P. Nali, Plates and Shells for Smart Structures: Classical and Advanced Theories for Modeling and Analysis, John Wiley & Sons, UK, 2011.
[8] A. Ghassemi, M. Hassan, S. Oveissi, Comparison of nonlinear Von Kármán and Cosserat theories in very large deformation of skew plates, Int. J. Adv. Struct. Eng. 10 (1) (2018) 73–84.
[9] P.G. Ciarlet, C. Mardare, A nonlinear shell model of Koiter's type, C. R. Math. 356 (2) (2018) 227–234.
[10] P.G. Ciarlet, C. Mardare, An existence theorem for a two-dimensional nonlinear shell model of Koiter's type, Math. Models Methods Appl. Sci. 28 (14) (2018) 2833–2861.
[11] J. Zhang, J. Xu, X. Yuan, H. Ding, D. Niu, W. Zhang, Nonlinear vibration analyses of cylindrical shells composed of hyperelastic materials, Acta Mech. Solida Sin. 32 (2019) 463–482.
[12] S. Abdulkerim, A. Dafnis, H.-G. Riemerdes, Experimental investigation of non-linear vibration of a thin rectangular plate, Int. J. Appl. Mech. 11 (6) (2019) 1950059.
[13] G.G. Sheng, X. Wang, The dynamic stability and nonlinear vibration analysis of stiffened functionally graded cylindrical shells, Appl. Math. Model. 56 (2018) 389–403.
[14] L. Benchouaf, E.H. Boutyour, E.M. Daya, M. Potier-Ferry, Non-linear vibrations of sandwich viscoelastic shells, C. R. Méc. 346 (4) (2018) 308–319.
[15] J. Altenbach, H. Altenbach, V. Eremeyev, On generalized cosserat-type theories of plates and shells: A short review and bibliography, Arch. Appl. Mech. 80 (1) (2010) 73–92, http://dx.doi.org/10.1007/s00419-009-0365-3.
[16] F. Alijani, M. Amabili, Non-linear vibrations of shells: A literature review from 2003 to 2013, Internat. J. Non-Linear Mech. 58 (2014) 233–257.
[17] V.M. Dolinskii, Calculations on loaded tubes exposed to corrosion, Chem. Pet. Eng. 3 (2) (1967) 96–97.
[18] P.A. Pavlov, B.A. Kadyrbekov, V.V. Borisevich, Uniform stress corrosion and corrosion cracking of structural steels, Sov. Mater. Sci. 21 (3) (1985) 248–251.
[19] E.M. Gutman, Mechano-Chemistry of Solid Surfaces, World Scientific, Singapore, 1994.
[20] I.G. Ovchinnikov, Yu.M. Pochtman, Calculation and rational design of structures subjected to corrosive wear (review), Mater. Sci. 27 (2) (1992) 105–116.
[21] E. Gutman, J. Haddad, R. Bergman, Stability of thin-walled high-pressure vessels subjected to uniform corrosion, Thin-Walled Struct. 38 (1) (2000) 43–52.
[22] E. Gutman, J. Haddad, R. Bergman, Stability of thin-walled high-pressure cylindrical pipes with non-circular cross-section and variable wall thickness subjected to non-homogeneous corrosion, Thin-Walled Struct. 43 (1) (2005) 23–32.
[23] R.M. Bergman, S.P. Levitsky, J. Haddad, E.M. Gutman, Stability loss of thin-walled cylindrical tubes, subjected to longitudinal compressive forces and external corrosion, Thin-Walled Struct. 44 (7) (2006) 726–729.
[24] J. Peng, C.-Y. Zhou, J.-L. Xue, X.-H. He, Safety assessment of pipes with multiple local wall thinning defects under pressure and bending moment, Nucl. Eng. Des. 241 (8) (2011) 2758–2765.
[25] Y.G. Pronina, Thermoelastic stress analysis for a tube under general mechano-chemical corrosion conditions, in: Proc. 4th Int. Conf. on Computational Methods for Coupled Problems in Science and Engineering, 2011, pp. 1408-1415.
[26] I. Elishahoff, G. Ghyselinck, Y. Miglis, Durability of an elastic bar under tension with linear or non-linear relationship between corrosion rate and stress, J. Appl. Mech. 79 (2) (2012) 021013.
[27] A. Eslami-Majd, A. Rahbar-Ranji, Free vibration analysis of corroded steel plates, J. Mech. Sci. Tech. 28 (6) (2014) 2081–2088.
[28] Y. Pronina, Analytical solution for the general mechano-chemical corrosion of an ideal elastic–plastic thick-walled tube under pressure, Int. J. Sol. Struct. 50 (2013) 3626–3633.
[29] S. Zhang, X. Pang, Y. Wang, K. Gao, Corrosion behaviour of steel with different microstructures under various elastic loading conditions, Corros. Sci. 75 (2013) 293–299.
[30] O.S. Sedova, Y.G. Pronina, Calculation of the optimal initial thickness of a spherical vessel operating in mechano-chemical corrosion conditions, in: International Conference Stability and Control Processes in Memory of V.I. Zubov (SCP), 2015, pp. 1-4.
[31] Y.G. Pronina, O.S. Sedova, S.A. Kabrits, On the applicability of thin spherical shell model for the problems of mechano-chemical corrosion, AIP Conf. Proc. 1648 (1) (2015) 300008.
[32] Y.G. Pronina, Mechano-chemical corrosion: modelling and analytical benchmarks for initial boundary value problems with unknown boundaries, Springer Proc. Math. Stat. 171 (2016) 301–307.
[33] E.M. Gutman, R.M. Bergman, S.P. Levitsky, On stability loss of a thin-walled spherical shell subjected to external pressure and internal homogeneous corrosion, in: ECCOMAS Congress, Greece, 2016, pp. 254-259.
[34] E.M. Gutman, R.M. Bergman, S.P. Levitsky, Influence of internal uniform corrosion on stability loss of a thin-walled spherical shell subjected to external pressure, Corros. Sci. 111 (2016) 212–215.
[35] H.-Q. Yang, Q. Zhang, S.-S. Tu, Y. Wang, Y.-M. Li, Y. Huang, A study on time-variant corrosion model for immersed steel plate elements considering the effect of mechanical stress, Ocean Eng. 125 (2016) 134–146.
[36] J. Awrejcewicz, A.V. Krysko, Some problems of analysis and optimization of plates and shells, J. Sound Vib. 264 (2) (2003) 343–376.
[37] V.A. Krysko, J. Awrejcewicz, A.V. Krysko, Thermo-Dynamics of Plates and Shells, Springer, Berlin, 2007.
[38] V.A. Krysko, J. Awrejcewicz, Chaos in Structural Mechanics, Springer, Berlin, 2008.
[39] J. Awrejcewicz, A.V. Krysko, T.V. Yakovleva, D.S. Zelenchuk, V.A. Krysko, Chaotic synchronization of vibrations of a coupled mechanical system consisting of a plate and beams, Lat. Am. J. Sol. Struct. 10 (1) (2013) 161–172.
[40] A.V. Krysko, J. Awrejcewicz, S.P. Pavlov, M.V. Zhigalov, V.A. Krysko, On the iterative methods of linearization, decrease of order and dimension of the Kármán-type PDEs, Sci. World J. 2014 (2014) 15.
[41] J. Awrejcewicz, V.A. Krysko, I.V. Papkova, A.V. Krysko, Deterministic Chaos in One Dimensional Continuous Systems, World Scientific, Singapore, 2016.
[42] J. Awrejcewicz, A.V. Krysko, I.V. Papkova, E.Y. Krylova, Chaotic dynamics of flexible beams driven by external white noise, Mech. Syst. Signal Process. 79 (2016) 225–253.
[43] E.Y. Krylova, I.V. Papkova, N.P. Erofeev, V.M. Zakharov, V.A. Krys'ko, Complex fluctuations of flexible plates under longitudinal loads with account for white noise, J. Appl. Mech. Tech. Phys. 57 (4) (2016) 714–719.

[44] E.Y. Krylova, T.V. Yakovleva, V.G. Bazhenov, Chaotic dynamics of flexible rectangular panels in white noise field, PNRPU Mech. Bull. 1 (2016) 82–92.
[45] T.V. Yakovleva, V.G. Bazhenov, V.A. Krysko, E.Y. Krylova, Contact interaction plates, reinforced by ribs, with gaps under the influence of white noise, PNRPU Mech. Bull. 4 (2015) 259–272.
[46] V.A. Krysko, I.V. Papkova, J. Awrejcewicz, E.Y. Krylova, A.V. Krysko, Non-symmetric forms of non-linear vibrations of flexible cylindrical panels and plates under longitudinal load and additive white noise, J. Sound Vib. 423 (2018) 212–229.
[47] A.E.H. Love, A Treatise on the Mathematical Theory of Elasticity, Dover Publications, New York, 1944.
[48] T. Kármán, Festigkeitsprobleme in maschinenbau, Encykle. D. Math. Wiss. 47 (1910) 311–385.
[49] M. Amabili, Nonlinear Mechanics of Shells and Plates: Composite, Soft and Biological Materials, Cambridge University Press, New York, USA, 2018.
[50] M. Amabili, Nonlinear Vibrations and Stability of Shells and Plates, Cambridge University Press, New York, USA, 2008.
[51] I.I. Vorovich, L.P. Lebedev, Nonlinear Theory of Shallow Shells, Springer, Berlin, 1999.
[52] L.P. Lebedev, I.I. Vorovich, Functional Analysis in Mechanics, Springer, New York, 2003.
[53] L.P. Lebedev, I.I. Vorovich, G.M.L. Gladwell, Functional Analysis: Application in Mechanics and Inverse Problems, Kluwer, Dordrecht, 2002.
[54] L.P. Lebedev, I.I. Vorovich, M.J. Cloud, Functional Analysis in Mechanics, Springer-Verlag, New York, 2013.
[55] I.I. Vorovich, On the existence of solutions in the non-linear theory of shells, News Acad. Sci. USSR 19 (4) (1955) 173–186.
[56] G. Frassoldati, G. Zanghirati, L. Zanni, New adaptive stepsize selections in gradient methods, J. Ind. Manag. Optim. 4 (2) (2008) 299–312.
[57] J.L. Lions, E. Maugenes, Non-Homogeneous Boundary Value Problems and Applications, Springer, Berlin, 1972.
[58] T.E. Schunk, Zur knienfestigkeit schwach gekrummter zylindrischer schalen, Ing. Arch. IV (1933) 394–414.
[59] V.V. Vlasov, General Theory of Shells and its Application in Engineering, NASA-TT-F-99, 1964.
[60] L.V. Kantorovich, V.I. Krylov, Approximate Methods of Higher Analysis, Interscience, New York, 1958.
[61] J. Awrejcewicz, V.A. Krysko, M.V. Zhigalov, A.V. Krysko, Contact interaction of two rectangular plates made from different materials with an account of physical nonlinearity, Int. J. Nonlinear Dyn. Chaos Eng. Sys. 85 (4) (2016) 2729–2748.
[62] A.V. Krysko, J. Awrejcewicz, M.V. Zhigalov, V.A. Krysko, On the contact interaction between two rectangular plates, Nonlinear Dynam. 91 (2) (2018) 1191–1211.
[63] W. Ramberg, A.E. Pherson, S. Levy, Normal pressure tests of rectangular plates, NACAT 849 (1942) 60.
[64] V.V. Bochkarev, V.A. Krysko, On an approach to the solution of geometrically nonlinear problems of the theory of plates, Izv. Univ. Constr. Archit. 10 (1981) 30–34.
[65] I.A. Birger, General solutions of some problems of the plasticity theory, Appl. Math. Mech. 15 (6) (1951) 765–770, (in Russian).
[66] S.A. Umanskii, On convergence of the method of variable stiffness parameters, Appl. Math. Mech. 44 (3) (1980) 577–584, (in Russian).
[67] V.F. Kirichenko, V.A. Krysko, On the existence of solution of one nonlinear the problem of thermoelasticity, Differ. Equ. XX (9) (1984) 1583–1588, (in Russian).